DOE/NV/10630-58

A SIMULATION OF THE TRANSPORT AND FATE OF RADON-222 DERIVED FROM THORIUM-230 LOW-LEVEL WASTE IN THE NEAR-SURFACE ZONE OF THE RADIOACTIVE WASTE MANAGEMENT SITE IN AREA 5 OF THE NEVADA TEST SITE

BY

F. TOM LINDSTROM
DAVID E. CAWLFIELD
MARY E. DONAHUE
DUDLEY F. EMER
GREGORY J. SHOTT

SPECIAL PROJECTS SECTION
ENVIRONMENTAL RESTORATION AND
TECHNOLOGY DEVELOPMENT DEPARTMENT

DECEMBER 1993

WORK PERFORMED UNDER
CONTRACT NO. DE-AC08-89NV10630

PREPARED BY
REYNOLDS ELECTRICAL & ENGINEERING CO., INC.
POST OFFICE BOX 98521
LAS VEGAS, NEVADA 89193-8521

DISCLAIMER

DOE/NV/10630-58
UC-721

A SIMULATION OF THE TRANSPORT AND FATE OF RADON-222 DERIVED FROM THORIUM-230 LOW-LEVEL WASTE IN THE NEAR-SURFACE ZONE OF THE RADIOACTIVE WASTE MANAGEMENT SITE IN AREA 5 OF THE NEVADA TEST SITE

BY

F. TOM LINDSTROM
DAVID E. CAWLFIELD
MARY E. DONAHUE
DUDLEY F. EMER
GREGORY J. SHOTT

SPECIAL PROJECTS SECTION
ENVIRONMENTAL RESTORATION AND
TECHNOLOGY DEVELOPMENT DEPARTMENT

DECEMBER 1993

WORK PERFORMED UNDER
CONTRACT NO. DE-AC08-89NV10630

PREPARED FOR
U.S. DEPARTMENT OF ENERGY
NEVADA OPERATIONS OFFICE

PREPARED BY
REYNOLDS ELECTRICAL & ENGINEERING CO., INC.
POST OFFICE BOX 98521
LAS VEGAS, NEVADA 89193-8521

ABSTRACT

U.S. Department of Energy (DOE) Order 5820.2A (DOE, 1988) requires performance assessments on all new and existing low-level radioactive waste (LLW) disposal sites. An integral part of performance assessment is estimating the fluxes of radioactive gases such as radon-220 and radon-222. Data needs pointed out by mathematical models drive site characterization. They provide a logical means of performing the required flux estimations.

Thorium-230 waste, consisting largely of thorium hydroxide and thorium oxides, has been approved for disposal in shallow trenches and pits at the LLW Radioactive Waste Management Site in Area 5 of the Nevada Test Site. A sophisticated gas transport model, CASCADR8 (Lindstrom et al., 1992b), was used to simulate the transport and fate of radon-222 from its source of origin, nine feet below a closure cap of native soil, through the dry alluvial earth, to its point of release into the atmosphere

CASCADR8 is an M-chain gas-phase radionuclide transport and fate model. It has been tailored to the site-specific needs of the dry desert environment of southern Nevada. It is based on the mass balance principle for each radionuclide and uses gas-phase diffusion as well as barometric pressure-induced advection as its main modes of transport. CASCADR8 uses both reversible and irreversible sorption kinetic rules as well as the usual classical Bateman (1910) M-chain decay rules for its kinetic processes.

Worst case radon-222 gas-phase concentrations, as well as surface fluxes, were estimated over 40 days. The maximum flux was then used in an exposure assessment model to estimate the total annual dose equivalent received by a person residing in a standard 2500-square-foot house with 10-foot walls. It was found that the predicted total committed effective dose equivalent (H_E) is 4×10^{-11} rem per year. The estimated H_E is many orders of magnitude less than the allowable limit of 0.025 rem per year for DOE waste disposal operations and 0.100 rem per year for inadvertent intruders.

CONTENTS

APPENDICES

FIGURES

FIGURES (CONTINUED)

TABLES

ACKNOWLEDGEMENT

The authors wish to thank Herb Sequera and Juanita Kuhn of Reynolds Electrical & Engineering Co., Inc., Administrative Services Department, for their invaluable help in typing, proofreading, and assembling this document.

1.0 INTRODUCTION

U.S. Department of Energy (DOE) Order 5820.2A (DOE, 1988) requires performance assessments on all new and existing LLW disposal sites. An integral part of performance assessment is estimating the fluxes of radioactive gases such as radon-220 and radon-222. Mathematical models, which in themselves point out data needs and therefore drive site characterization, provide a logical means of performing the required flux estimations. Very few mathematical models of noble gas transport from the spatial point of origin in the low-level waste repository through the surrounding soil and closure cap with subsequent release to the atmosphere seem to exist (Nazaroff, 1992). This model includes the diffusion and barometric pressure-induced advection of an M-chain of radionuclides. The parent material is assumed to be buried somewhere between the soil-atmosphere interface and the water table some 240 meters below the surface. The usual Bateman decay mechanics are included with each radionuclide. Both linear reversible sorption kinetics and linear irreversible sorption kinetics are assumed for each radionuclide.

Our model is called CASCADR8. The detailed physics-based model assumptions and mathematical methods used to obtain the numerical solution are given in Lindstrom et al. (1992a and 1992b). The homogeneous porous medium version of this gas-phase model (CASCADR8) was successfully used to predict the transport and fate of radon-220 in the same dry NTS porous medium in Lindstrom et al. (1992c). CASCADR9 allows for direct barometric pressure drive (real weather data) while CASCADR8 requires the user to tailor the barometric pressure function as a series of trigonometric sine and cosine waves (up to 15 components). CASCADR9 can easily be run in the homogeneous porous medium mode.

2.0 THORIUM-230 LOW-LEVEL WASTE

In the spirit of performance assessment, CASCADR8 was used to simulate the transport and fate of radon-222, which is derived from radium-226 (a metal), and is the second radionuclide in the thorium chain of the uranium series. This document illustrates thorium waste characterization, its subsequent burial at the Area 5 Radioactive Waste Management Site (RWMS), and the resultant worst case surface flux scenario for a 10,000 year period of time. Figure 2.0.1 lists the uranium series and relates the position of thorium-230 in the series.

2.1 Thorium-230 Waste Stream Summary

The Westinghouse Materials Co. of Ohio (WEMCO) thorium waste stream currently approved for disposal at the Nevada Test Site (NTS) consists of thorium hydroxide and thorium oxides packaged from feed materials stored in Fernald, Ohio. Table 2.1.1 summarizes the thorium-230 waste currently being received from WEMCO.

Table 2.1.1 Thorium-230 Waste Stream Summary

approximate number of containers	1600
container type	48-gallon drums in 55-gallon overpacks
estimated total volume of drums	339 m^3
estimated total volume of waste	291 m^3
total mass of waste	288,774 kg = 63,767 lbs
total mass Th-230 (impurity)	99 g
total activity	2.0 Ci
specific activity	6.9 (μCi/kg)
mean activity/drum volume	5.9 mCi/m^3
mean activity/waste volume	6.9 mCi/m^3
mean mass/drum	180 kg x 1,600 = 288,000 kg
mean activity/drum	1.2 mCi = 2Ci/1,600

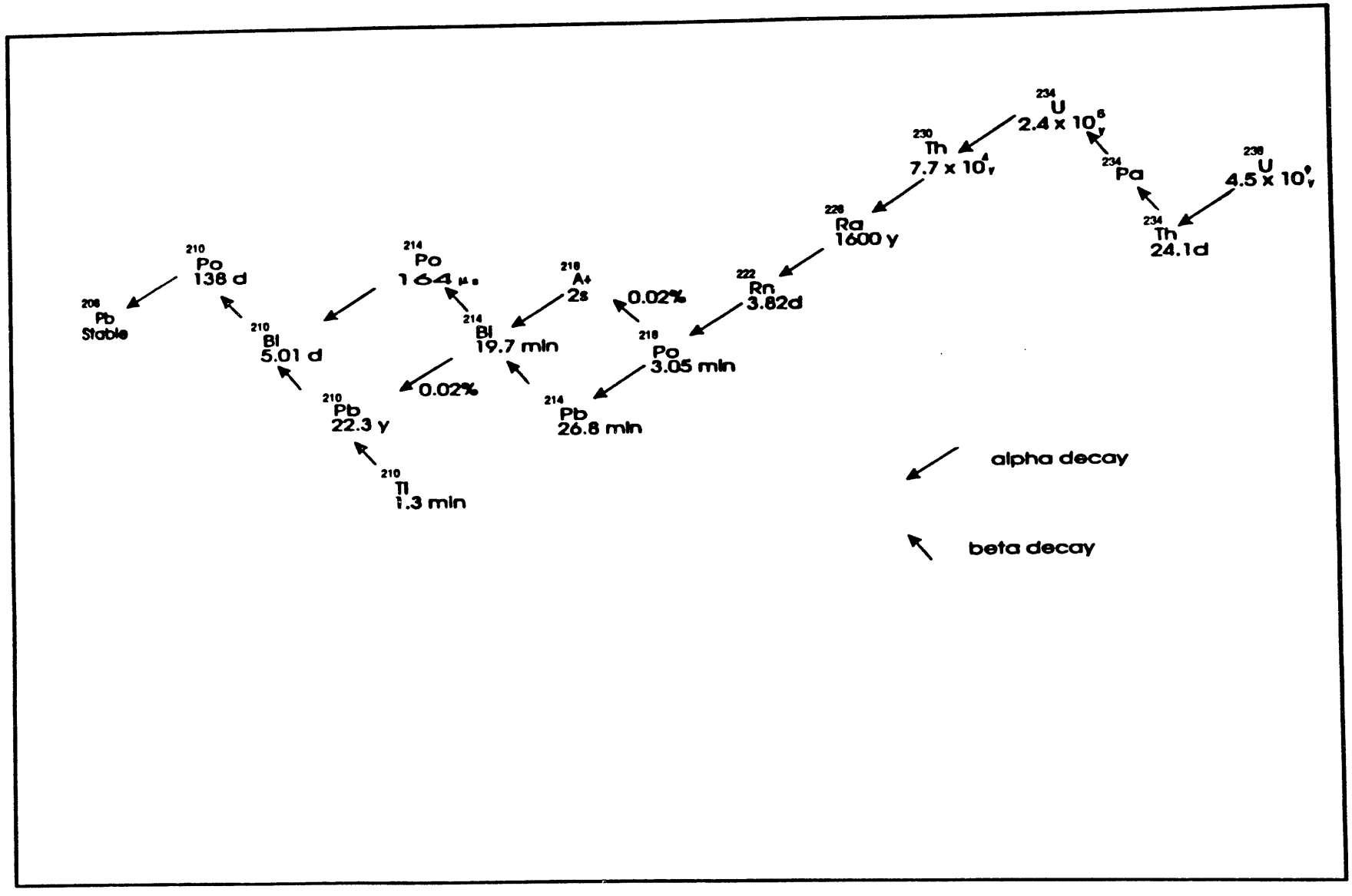

Figure 2.0.1 Uranium-238 Decay Chain.

2.2 Characterization of Source of Radionuclides

Table 2.2.1 details the thorium-230 decay-chain physical data necessary to characterize the source term for radon-222. A separate chemical mass-based Bateman (1910) decay-chain model called CHAIN1, that is detailed in Appendix B, of Lindstrom et al. (1992b), was run to simulate a period of 10,000 years. Figure 2.2.1 shows the ingrowth of radium-226 in grams given 99 grams of thorium-230 at time t=0. Table 2.2.2 gives the chemical mass of each radionuclide in the thorium chain beginning with thorium-230 at time t=0 seconds (column 2) and cascading down through radium-226 (column 3).

Table 2.2.1 Thorium-230 Chain Data (Brown and Firestone, 1986)

Radionuclide	Half-Life	Atomic Mass (gm/mole)	Branching Ratio	Specific Activity (pCi/gm)
thorium-230	7.7×10^4 yrs	230	1.0	2.0202×10^{10}
radium-226	1,600 yrs	226	1.0	0.989×10^{12}
radon-222	3.8235 days	222	1.0	1.6377×10^{17}

The mass of radium-226 currently available at the 10,000-year mark (3.15576×10^{12} sec) is computed to be 1.86 grams. By 10,000 years, the peak in the radium-226 ingrowth curve is achieved. Figure 2.2.1 shows the radium-226 ingrowth from the 99 grams of thorium-230. Thus, it was assumed that 1.86 gm of radium-226 will be constantly available in the 99 gm of low-level thorium waste. Table 2.2.3 illustrates the data file used in CASCADR8 to make the simulation run. The Area 5 RWMS Operations Manager decided to stack the thorium waste packages in Trench 3 in two rectangular parallelepiped nests 768 cm wide, 1,377 cm long, and 490 cm high. Because the bottom of Trench 3 is 25 feet below grade, the waste will be 9 feet below grade when fully stacked. The source term for radium-226 was then assumed to exist in the worst possible condition; namely, radium-226 is instantaneously and uniformly released within the above-defined volume. Thus, the constant source rate function

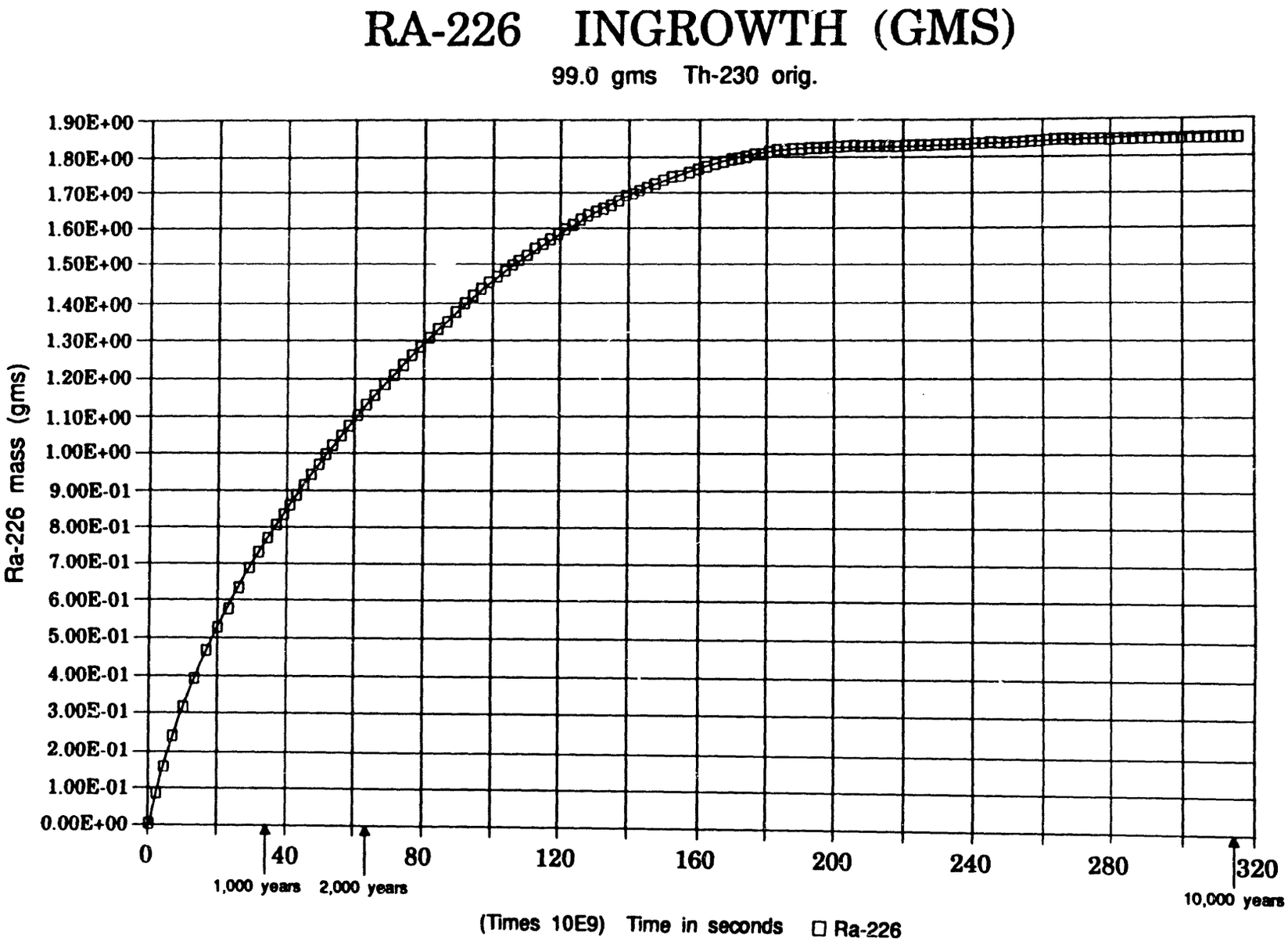

Figure 2.2.1 Ingrowth of Ra-226 from 99 grams of Th-230 at time t=0 years.

Table 2.2.2 Chemical Mass Form of the Thorium-230/Radium-226 Bateman Decay-Chain

```
XMASSO   =  99.000000000000000
DT       =  3.155760000000000E+009
NEVAL    =  101
```

HALF-LIVES AND DECAY CONSTANTS TABLE

```
 1     2.429935200000000E+012  2.851927903262605E-013
 2     5.049216000000000E+010  1.372490303445129E-011
```

CHAIN COEFFICIENTS

```
1   .100000E+01     .000000E+00     .000000E+00     .000000E+00     .000000E+00
2   .212202E-01    -.212202E-01     .000000E+00     .000000E+00     .000000E+00
```

MASTER EVALUATION LOOP

Time\Sec	Th-230 (gm)	Ra-226 (gm)
.000000E+00	.990000E+02	.337502E-15
.315576E+10	.989109E+02	.856427E-01
.631152E+10	.988220E+02	.167578E+00
.946728E+10	.987331E+02	.245963E+00
.126230E+11	.986442E+02	.320949E+00
.157788E+11	.985555E+02	.392680E+00
.189346E+11	.984668E+02	.461293E+00
.220903E+11	.983783E+02	.526921E+00
.252461E+11	.982898E+02	.589691E+00
.284018E+11	.982013E+02	.649724E+00
.315576E+11	.981130E+02	.707135E+00
.347134E+11	.980247+E02	.762036E+00
.378691E+11	.979366E+02	.814534E+00
.410249E+11	.978484E+02	.864730E+00
.441806E+11	.977604E+02	.912723E+00
.473364E+11	.976725E+02	.958605E+00
.504922E+11	.975846E+02	.100247E+01
.536479E+11	.974968E+02	.104439E+01
.568037E+11	.974091E+02	.108446E+01
.599594E+11	.973215E+02	.112276E+01
.631152E+11	.972339E+02	.115936E+01
.662710E+11	.971465E+02	.119433E+01
.694267E+11	.970591E+02	.122775E+01
.725825E+11	.969718E+02	.125967E+01
.757382E+11	.968845E+02	.129016E+01
.788940E+11	.967974E+02	.131929E+01
.820498E+11	.967103E+02	.134710E+01
.852055E+11	.966233E+02	.137366E+01
.883613E+11	.965364E+02	.139902E+01
.915170E+11	.964495E+02	.142323E+01

Table 2.2.2 Chemical Mass Form of the Thorium-230/Radium-226 Bateman Decay-Chain (Cont.)

MASTER EVALUATION LOOP (Con.t)

Time\Sec	Th-230 (gm)	Ra-226 (gm)
.946728E+11	.963628E+02	.144634E+01
.978286E+11	.962761E+02	.146840E+01
.100984E+12	.961895E+02	.148944E+01
.104140E+12	.961029E+02	.150952E+01
.107296E+12	.960165E+02	.152867E+01
.110452E+12	.959301E+02	.154693E+01
.113607E+12	.958438E+02	.156435E+01
.116763E+12	.957576E+02	.158095E+01
.119919E+12	.956714E+02	.159678E+01
.123075E+12	.955854E+02	.161186E+01
.126230E+12	.954994E+02	.162622E+01
.129386E+12	.954135E+02	.163990E+01
.132542E+12	.953276E+02	.165293E+01
.135698E+12	.952419E+02	.166533E+01
.138853E+12	.951562E+02	.167713E+01
.142009E+12	.950706E+02	.168836E+01
.145165E+12	.949851E+02	.169904E+01
.148321E+12	.948996E+02	.170919E+01
.151476E+12	.948143E+02	.171884E+01
.154632E+12	.947290E+02	.172800E+01
.157788E+12	.946438E+02	.173670E+01
.160944E+12	.945586E+02	.174496E+01
.164100E+12	.944735E+02	.175280E+01
.167255E+12	.943886E+02	.176023E+01
.170411E+12	.943036E+02	.176727E+01
.173567E+12	.942188E+02	.177394E+01
.176723E+12	.941341E+02	.178025E+01
.179878E+12	.940494E+02	.178622E+01
.183034E+12	.939648E+02	.179187E+01
.186190E+12	.938802E+02	.179720E+01
.189346E+12	.937958E+02	.180223E+01
.192501E+12	.937114E+02	.180698E+01
.195657E+12	.936271E+02	.181146E+01
.198813E+12	.935429E+02	.181567E+01
.201969E+12	.934587E+02	.181963E+01
.205124E+12	.933746E+02	.182334E+01
.208280E+12	.932906E+02	.182683E+01
.211436E+12	.932067E+02	.183010E+01
.214592E+12	.931229E+02	.183316E+01
.217747E+12	.930391E+02	.183601E+01
.220903E+12	.929554E+02	.183867E+01
.224059E+12	.928718E+02	.184115E+01
.227215E+12	.927882E+02	.184345E+01
.230370E+12	.927048E+02	.184558E+01
.233526E+12	.926214E+02	.1847454E+01
.236682E+12	.925380E+02	.184936E+01

Table 2.2.2 Chemical Mass Form of the Thorium-230/Radium-226 Bateman Decay-Chain (Cont.)

MASTER EVALUATION LOOP (Con.t)

Time\Sec	Th-230 (gm)	Ra-226 (gm)
.239838E+12	.924548E+02	.185102E+01
.242994E+12	.923716E+02	.185254E+01
.246149E+12	.922885E+02	.185392E+01
.249305E+12	.922055E+02	.185517E+01
.252461E+12	.921226E+02	.185630E+01
.255617E+12	.920397E+02	.185731E+01
.258772E+12	.919569E+02	.185820E+01
.261928E+12	.918742E+02	.185899E+01
.265084E+12	.917915E+02	.185967E+01
.268240E+12	.917089E+02	.186025E+01
.271395E+12	.916264E+02	.186073E+01
.274551E+12	.915440E+02	.186112E+01
.277707E+12	.914617E+02	.186143E+01
.280863E+12	.913794E+02	.186165E+01
.284018E+12	.912972E+02	.186178E+01
.287174E+12	.912150E+02	.186185E+01
.290330E+12	.911330E+02	.186183E+01
.293486E+12	.910510E+02	.186175E+01
.296641E+12	.909691E+02	.186160E+01
.299797E+12	.908873E+02	.186139E+01
.302953E+12	.908055E+02	.186111E+01
.306109E+12	.907238E+02	.186078E+01
.309264E+12	.906422E+02	.186039E+01
.312420E+12	.905607E+02	.185994E+01

Table 2.2.3 Data File Used in CASCADR8 for Simulating Thorium-230 Waste

```
Datafile is (C9230102.DAT)  Transport of (Radon 222) chain,
starting with Ra226 (from the Thorium230 chain) as the parent.
NOAA, NTS Frenchman Flat data.

Run 2: Run with *new* baro.dat (revised Nov ' 92).
       400 day run.

       Note -- Comment lines now end with "$" in column 1

$
SET OF FLAGS: NFLAG(I)
0,0,0,0,0,0,1,1,1,0
NLAYERS   NODES   NUCS  NOUT
1         401     1     600
Spacing is 'A' for Absolute, 'R' for Relative
'R'
ZOFF, then NM1 spacingS for DZZ
0.0D0
1.0D0 1.5D0 2.0D0 2.5D0 3.0D0 5.0D0 7.5D0 1.0D1
7.5D0 1.0D1 1.0D1 1.5D1 1.5D1 2.0D1
```

Table 2.2.3 Data File Used in CASCADR8 for Simulating Thorium-230 Waste (Cont.)

```
05*2.0D1
2.0D1
1.5D1 1.0D1 7.5D0 7.5D0 5.0D0 2.5D0 2.5D0 5.0D0
1.0D1 1.5D1 2.0D1
19*2.0D1
2.0D1 1.5D1 1.0D1 5.0D0 5.0D0
1.0D1 1.5D1 2.0D1
127*2.0D1
2.0D1 3.0D1 4.0D1 5.0D1 6.0D1 7.0D1 8.0D1 9.0D1 1.0D2
207*1.0D2
Spacing for layers: 'A' for absolute, 'R' for relative
'A'
BOTTOM DEPTH FOR N-1 LAYERS; LAST ONE IS DEPTH OF WATER TABLE, NOT LISTED
NDEP; then 'N' for nodes or 'Z' for actual depths
08 'Z'
PRINT AT THESE NODAL POSITIONS
0.0D0, 1.0D2, 2.0D2, 2.75D2, 7.60D2, 1.6D3, 3.2D3, 2.44D4
INITIAL TIME: T0
0.0D0
FINAL TIME: TIME
3.456D+7
NUMBER OF PRINT TIMES: NPRT
360
DT
60.0D0
PARTDN    EPS    KAPPA
2.6       0.37   4.00D-8
EPSIN,EPSOT
0.37, 1.0
DSO1
0.10
DSP1   ONE ROW FOR EACH LAYER
0.05
DSOT1
1.00
FREV1
0.10
FIRR1
0.10
KEQ1
0.00
THALF[0..MNUCS]
5.05D+10, 3.305D+5
AM[0..MNUCS]
226.D0, 222.D0
SA[0..MNUCS]
0.989D12, 1.5377D17
LTIRR1    ONE ROW FOR EACH LAYER
0.0
AREA
1.0D+4
COT1
0.0
CIN1
1.000D-28
DXIN
100.0D0
DXOUT
100.0D0
TAIR,     RG,          MASSA,     GRAV,     RHOWAT
2.93D+2, 8.3143D+7,   29.0D0,    9.8D+2,   1.0D0
PA AND NPRES
```

Table 2.2.3 Data File Used In CASCADR8 for Simulating Thorium-230 Waste (Cont.)

```
917. 0D0, 1
POC'S FROM 1 TO 15
+0.0000D0, +0.0000D0, +0.0000D0, -0.0000D0, +0.0000D0
+0.0000D0, -0.0000D0, +0.0000D0, -0.0000D0,  0.0000D0
 0.0000D0,  0.0000D0,  0.0000D0,  0.0000D0,  0.0000D0
POS'S FROM 1 TO 15
-0.0000D0, +0.0000D0, +0.0000D0, +0.0000D0, -0.0000D0
-0.0000D0, +0.0000D0, -0.0000D0, +0.0000D0,  0.0000D0
 0.0000D0,  0.0000D0,  0.0000D0,  0.0000D0,  0.0000D0
PERIODS OF EACH COMPONENT IN SECS.
1.0000D+0, 1.0000D+0, 1.0000D+0, 1.0000D+0, 1.0000D+0
1.0000D+0, 1.0000D+0, 1.0000D+0, 1.0000D+0, 1.0000D+0
1.0000D+0, 1.0000D+0, 1.0000D+0, 1.0000D+0, 1.0000D+0
Number of Source Regions; 'N' for nodes, 'Z' for depths.
01      'Z'
INITIAL DISTRIBUTION DATA
00      0.000D0   2.440D4   1.000D-28,   0.0D0
01      2.750D2   7.600D2   1.000D-28,   5.0480D-20
```

required by CASCADR8 is obtained as

$$S_{SP}(x) = \left(\frac{1.86\ \text{gm}}{5.057 \times 10^{8}\ \text{cm}^3}\right) \frac{(0.693)}{5.0492 \times 10^{10}\ \text{sec}} = 5.048 \times 10^{-20}\ . \quad (\text{gm/cm}^3/\text{sec}) \quad (2.2.1)$$

Having the constant-in-time source rate function defined as per above, the top of the source is placed nine feet below grade and the bottom of the source is 25 feet below grade. In the following simulation the water table is 240 meters below grade. A cap of nine feet of native soil (gas permeability of 4 Darcies) is put over the top of the waste to bring the soil-atmosphere interface up to grade. No credit is taken for any of the waste packaging material.

2.3 Radon-222 Diffusion Coefficient, Sorption Coefficients

The diffusion coefficient for radon-222 in still, dry air is approximately 0.1 cm^2/sec (Nazaroff, 1992). Our current site characterization project in Area 5 indicates that the surface soils have an average porosity of 0.37 cm^3/cm^3 (site characterization report in progress). A tortuosity of 0.5 seems reasonable (Nazaroff, 1992), considering surface

moisture contents are approximately 0.05 to 0.07 cm^3/cm^3 (site characterization report in process). Therefore, the radium-222 diffusion coefficient in the dry desert alluvium is set at 0.0225 cm^2/sec. This value provides a conservative estimate of radium-222 diffusion in the dry desert soil on the NTS.

It is assumed that radon-222 does not bind to any of the dry alluvial surfaces. Nazaroff (1992) does show that in the presence of pore water, radon-222 is appreciably retarded in its diffusion due to the partitioning into and diffusion through water films around the particles. Therefore, it is a conservative assumption that radon-222 is nonbinding.

2.4 Barometric Pressure Data

Since CASCADR9 uses either real barometric pressure data or "homemade" pressure data made up from a linear combination of up to 15 sinusoids and cosinusoids, real barometric pressure data was selected for use. Thus, pressure data from MEDA 5 (a NOAA weather station in Area 5 of NTS) collected over a two year period were obtained from Dr. Daryl Randerson (1992) of the Nuclear Support Services Department of USDOE/NV. The 15 minute barometric pressure data spanned a time of two years (730 days). It did contain numerous omissions (gaps in the sequence) and therefore required the writing of a Lagrange cubic spline (Press et al. 1986) to fill in the missing data. Julian dates are used in the data file for reading the barometric pressure. Thus, the 40-day simulation runs found in this report used real 15 minute barometric pressure data and Lagrange smooth cubic spline estimated 15 minute barometric pressure in millibars (mb) beginning at day 110 (midnight = 0, time) and ending at midnight on day 150. Figure 2.4.1 shows the actual surface barometric pressure in mb used for the 40-day simulation runs.

2.5 Other Environmental and Boundary Data

The air temperature is fixed at 20°C (293°K). Since CASCADR9 is an isothermal model, the soil temperature is also assumed to be constant at 20°C . Later versions of CASCADER will relax the isothermal requirements.

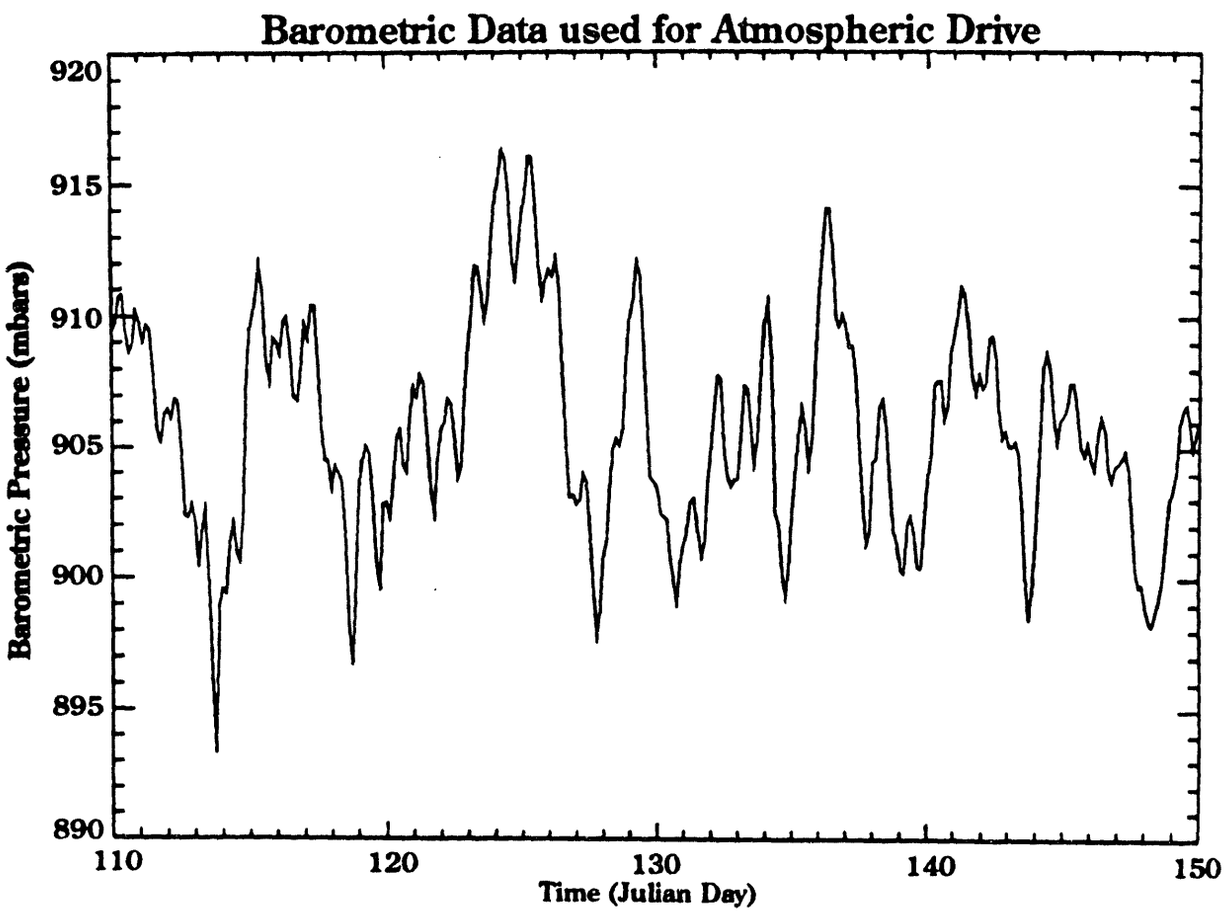

Figure 2.4.1 Real barometric pressure data used in the 40-day simulations.

The radon-222 atmospheric concentration is fixed at zero with a screen height of 100 cm above the soil-atmosphere interface. The radon-222 flux at the surface is calculated accordingly. The cumulative radon-222 flow is defined as

$$\text{Cum}(t) = A\int_0^t \underset{\sim}{q}\Big|_{z=0} \cdot \hat{n}\, d\tau \quad , \tag{2.5.1}$$

where A is fixed at 10^4 cm^2 (one square meter of surface area).

3.0 RESULTS OF 40-DAY SIMULATION RUNS

3.1 Base Case

The base case means the usual configuration of stacking the drums one on top of the other and thereby generating a "thick" source 16 feet thick. Allowed here is about three inches of native soil between each layer or tier of drums. The top of the waste region is then nine feet below grade (-2.8 m) while the bottom of the waste region is 25 feet below grade (-7.6 m).

Figure 3.1.1 shows the flux of radon-222 off the surface immediately above the buried low-level waste. The actual chemical flux in gm/cm^2-sec of radon-222 has been multiplied by the specific activity of radon-222 in pCi/gm to obtain the radon-222 activity flux in pCi/cm^2-sec. National Emission Standards for Hazardous Airborne Pollutants (NESHAP) requires that the surface flux of radon-222 be less than 2×10^{-3} pCi/cm^2-sec. The background source of radon-222 (naturally occurring radium-226 in the desert alluvium) has been artificially lowered by roughly ten orders of magnitude so as to not confound the surface flux stemming from the buried manmade source. The 24-hour average surface flux of radon-222 on day 40 is -3.762×10^{-2} pCi/cm^2-sec. The minus sign indicates a loss of surface flux to the atmosphere. This configuration is clearly in violation of NESHAP.

Figure 3.1.2 shows the cumulative flow of radon-222 off the surface of one square meter of soil-atmosphere interface. The "straight line" character, appearing after day 10, shows the steady-state diffusive loss character. The steady-state diffusion controlled loss is $\sqrt{t}$ for large time t values and when plotted on semi-log paper, the character is quite linear or straight line looking. Figure 3.1.3 shows the radon-222 air-phase concentration in pCi/cm^3 at the atmosphere-alluvium interface. Some of the daily peaks reach about 200 pCi/cm^3. While some of the low values dip down to about 5 pCi/cm^3.

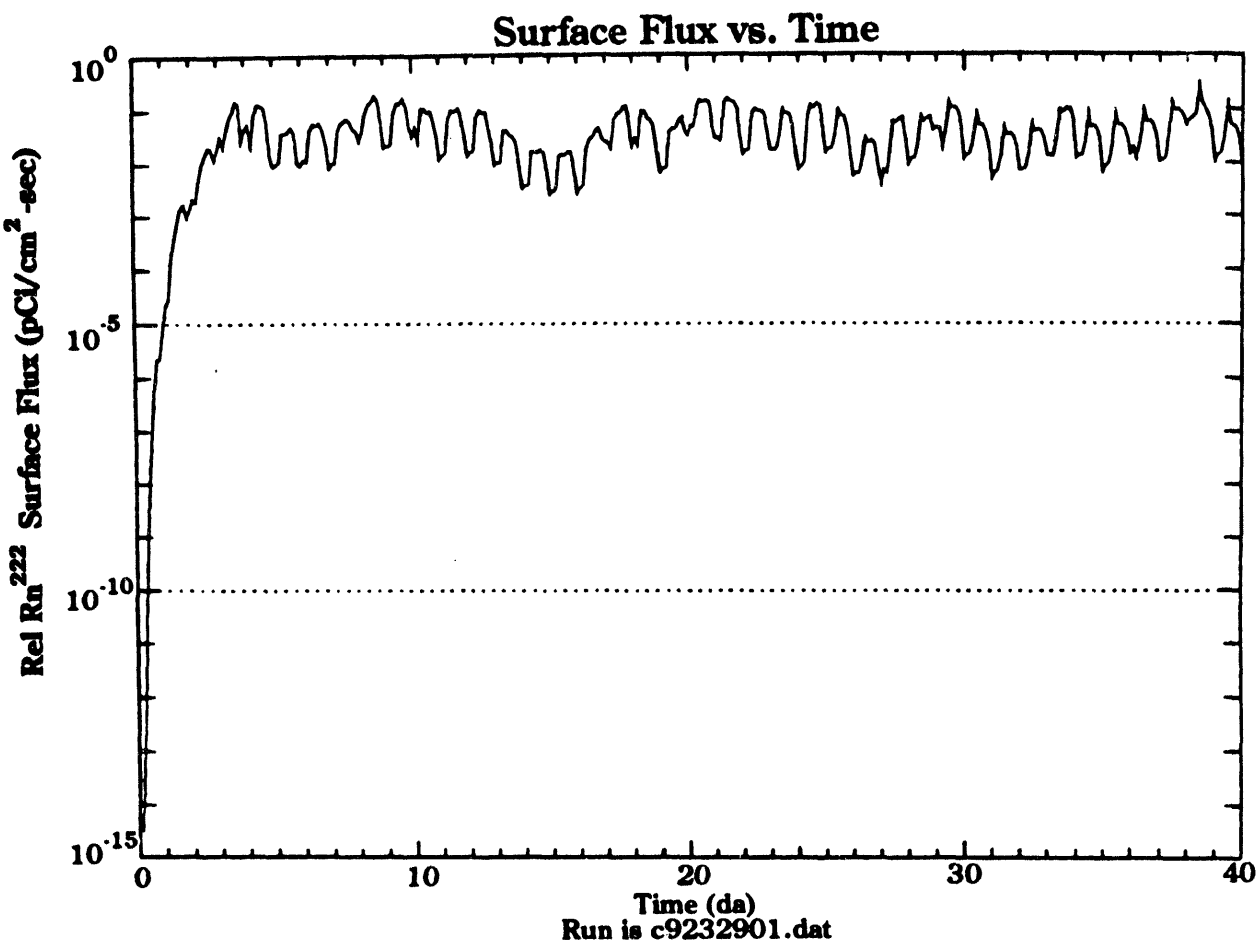

Figure 3.1.1 Surface flux of radon-222 in pCi/cm^2-sec. Base case NESHAP requires the flux to be less than 2 x 10^{-3} pCi/cm^2-sec.

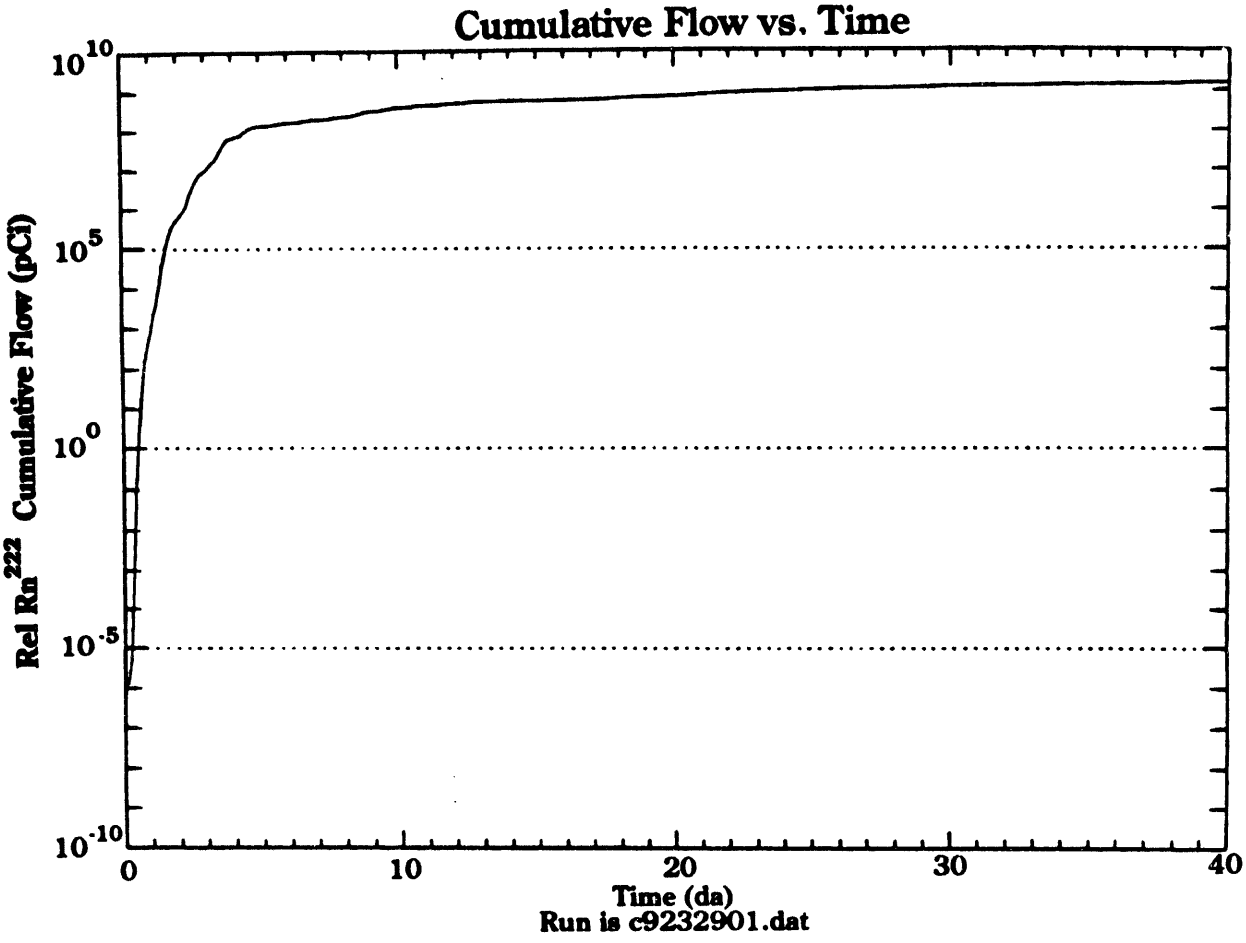

Figure 3.1.2 Cumulative radon-222 surface flux through one square meter of surface. Base case.

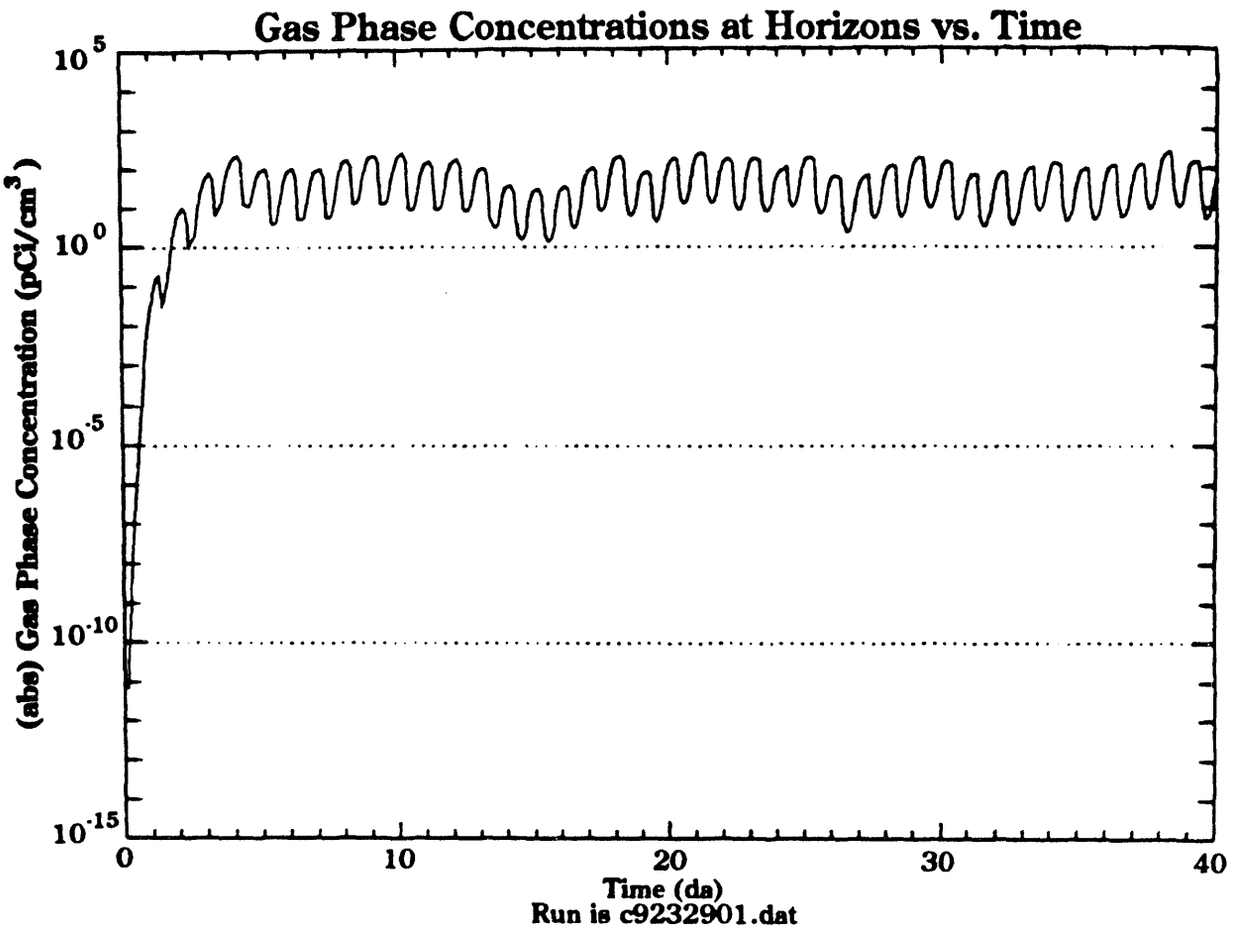

Figure 3.1.3 Radon-222 air concentration in pCi/cm^3 at the air-alluvium surface. Base case.

3.2 Alternative Burial Scenarios

Figure 3.1.1 clearly shows that the base case burial scenario results in a radon-222 flux at the surface exceeding the NESHAP standard by two orders of magnitude. Lindstrom et al. (1992b) used a later version of CASCADR8, a version which allows for layered porous media, in an engineering design study to assess the effects of changing the transport properties of a control layer over the waste, and changing the depth of burial of the manmade waste on the surface flux of radon-222. The work shows very clearly, the depth of burial is a crucial engineering design parameter with the surface flux of radon-222 appearing to fall off exponentially as the depth of burial increases. Thus, the following scenarios are presented as alternatives to the base case of waste burial where radon-222 transport and fate give real cause for concern.

The key change in this burial procedure from past procedure is that instead of stacking the waste packages in a "four-tier" fashion (either boxes or drums), a single tier or layer is assumed. This effectively reduces the thickness of the source by a factor of four. Even though the same mass and volume of waste is involved as the base case and the area increased by a factor of four, the added area is more than offset by the reduction in source region thickness. Appendix F of Cawlfield et al. (1993) details the mathematics, which for the case of purely diffusional transport, shows the non-linear effects of the source thickness on the radon-222 surface flux assuming a very dry homogeneous porous medium above and below the waste region.

In the following five depth of burial scenarios the source region concentration is assumed to be the same as the base case; namely,

$$S_{SP}(x) = 5.048 \times 10^{-20} \quad (gm/cm^3\text{-sec}). \quad (3.2.1)$$

The thickness of the source region is reduced to one meter (3.3 feet) in the following five scenarios:

Alternative 1 (X_T = 280 cm, X_B = 380 cm)

In this scenario the single tier source top is 280 cm below grade and its bottom 380 cm below grade. Figures 3.2.1 through 3.2.3 summarize the radon-222 surface flux as a function of time, the cumulative radon-222 surface flow per square meter as a function of time, and the radon-222 gas-phase concentration at the surface as a function of time. The simulation was made for 40 days. Comparison of Figures 3.1.1 the base case and 3.2.1 the shallowest depth of burial scenario in the suite of five depth of burial alternatives, shows that alternative one lies under the base case, but that NESHAP is still exceeded. There is no engineered cover over the waste, only the necessary 2.8 meters of native alluvium to bring the surface back to background grade. The surface flux has achieved steady-state about day 10.

Alternative 2 (X_T = 660 cm, X_B = 760 cm)

In this scenario the single tier source top is 660 cm below grade and its bottom 760 cm below grade. As per Figures 3.2.1 through 3.2.3, Figures 3.2.4 through 3.2.6 summarize the radon-222 surface flux time distribution, the cumulative radon-222 surface flow through 10^4 cm^2 of surface area, and the gas-phase radon-222 concentration at the alluvium-atmosphere interface over the same 40 days of real barometric pressure data used in alternative one. Comparison of Figures 3.2.1 and 3.2.4 clearly shows that the radon-222 surface flux peaks are very close to the NESHAP level of 2×10^{-3} pCi/cm^2-sec. A dramatic reduction in surface flux is seen with the increase in depth of burial. No engineered cap is used, only the 6.6 meters of native soil as a backfill material over the top of the waste region.

Alternative 3 (X_T = 1,120 cm, X_B = 1,220 cm)

In this scenario the single tier source top is placed at 1,120 cm below grade while the bottom of the source lies 1,220 cm below grade. Figures 3.2.7 through 3.2.9 summarize the same attributes of the model as the first and second sets of figures in

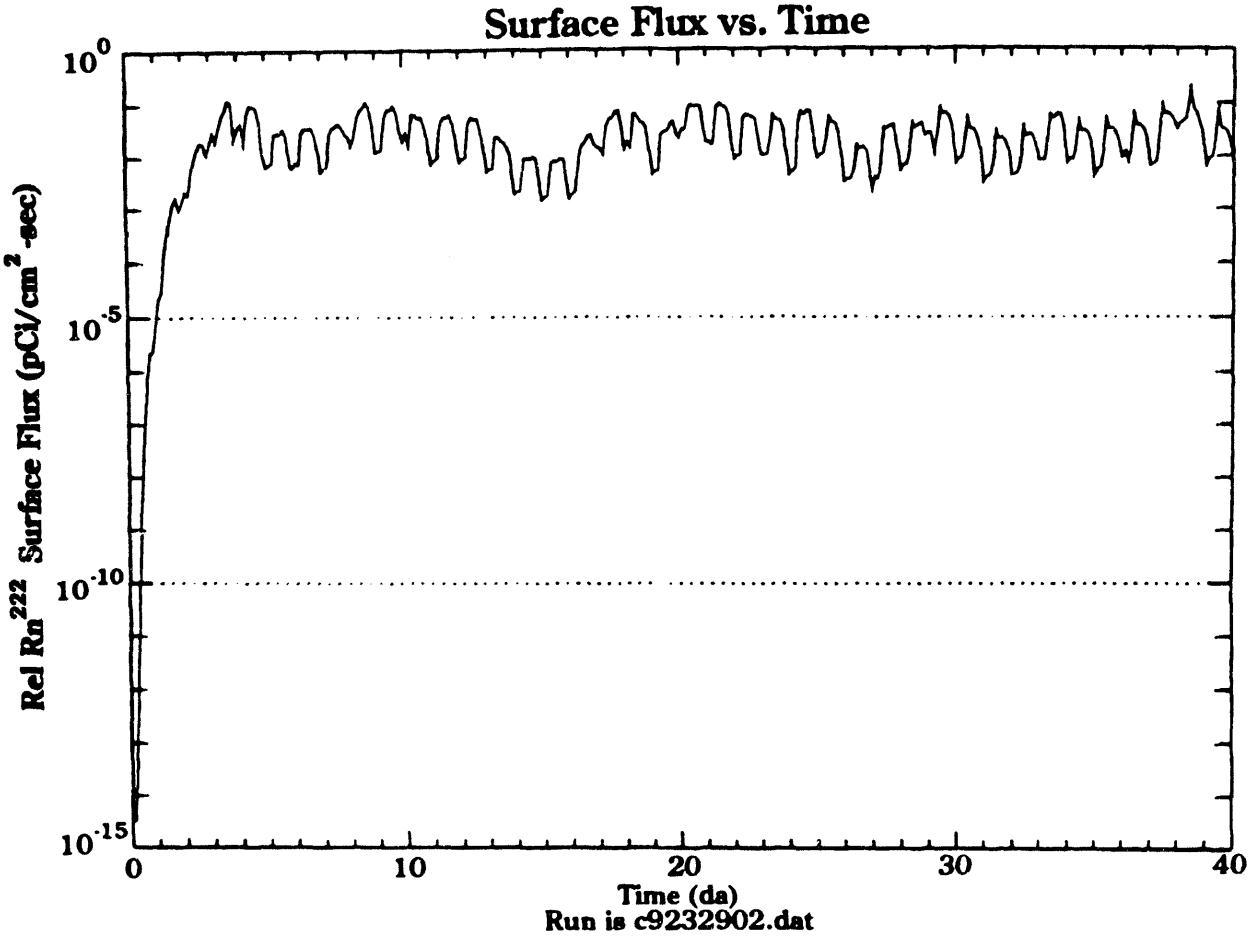

Figure 3.2.1 Alternative 1. Radon-222 surface flux (pCi/cm^2-sec).

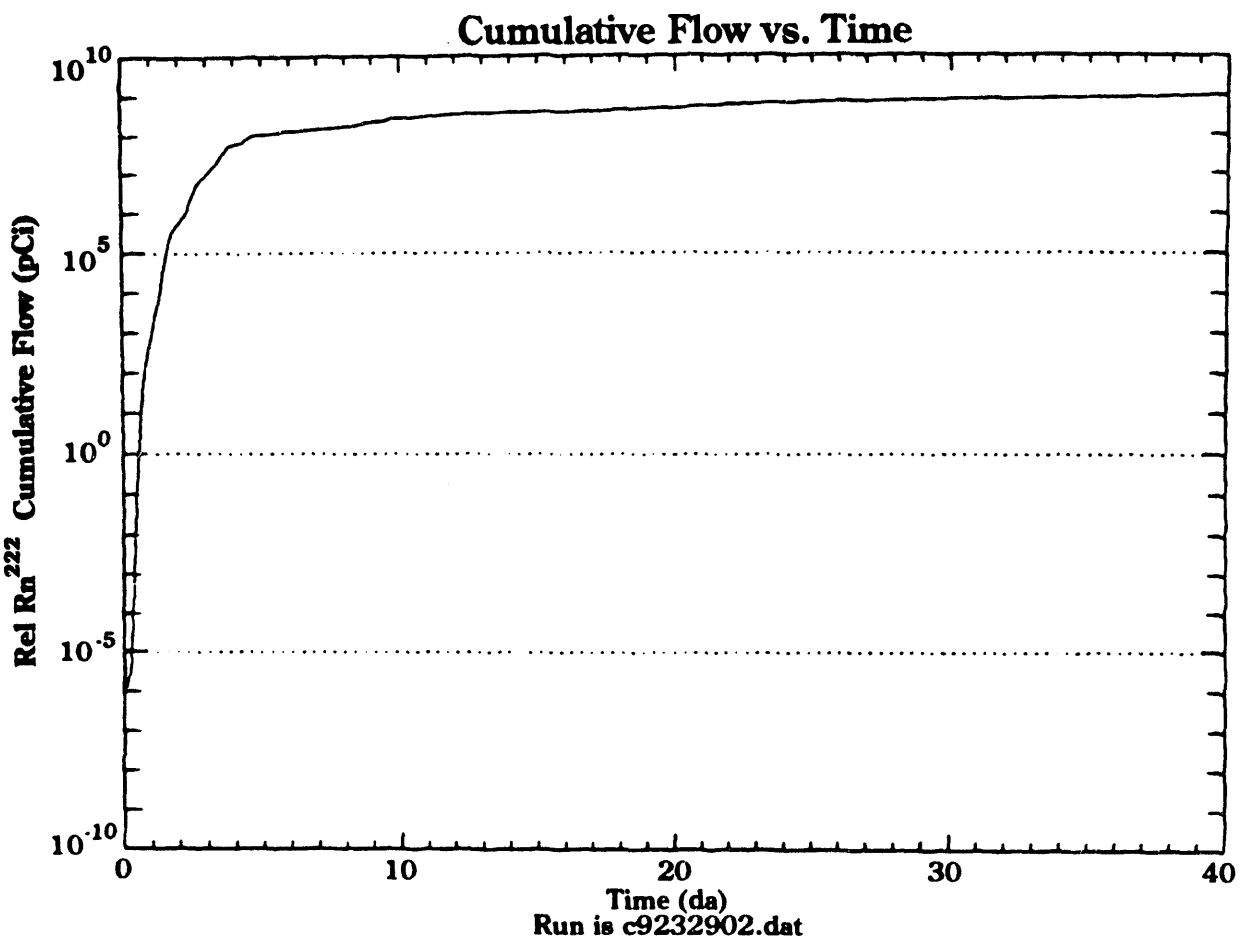

Figure 3.2.2 Alternative 1. Cumulative surface flow of radon-222 through 10^4 cm^2 of surface area (pCi).

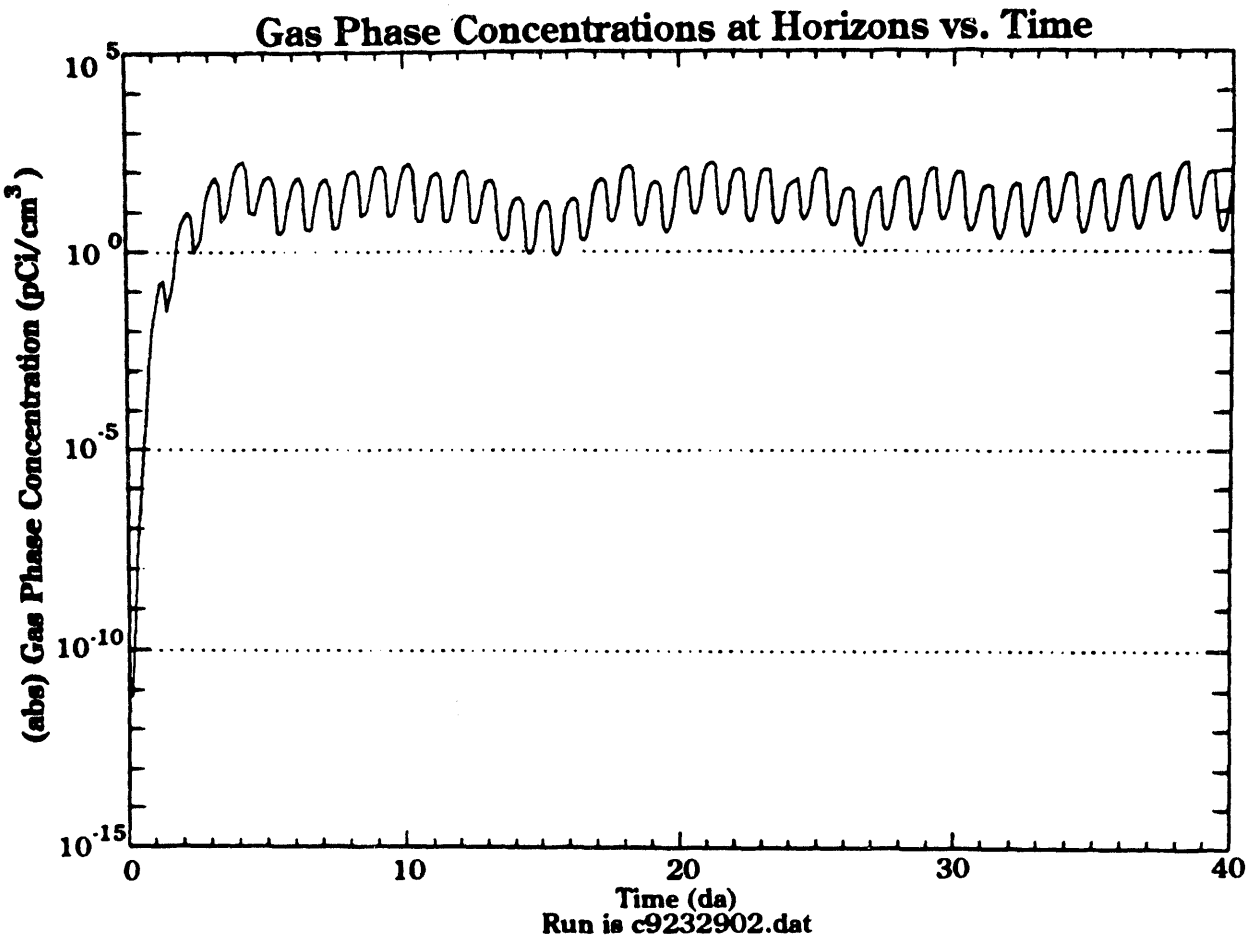

Figure 3.2.3 Alternative 1. Radon-222 gas-phase concentration (pCi/cm^3) at the alluvium-atmosphere interface.

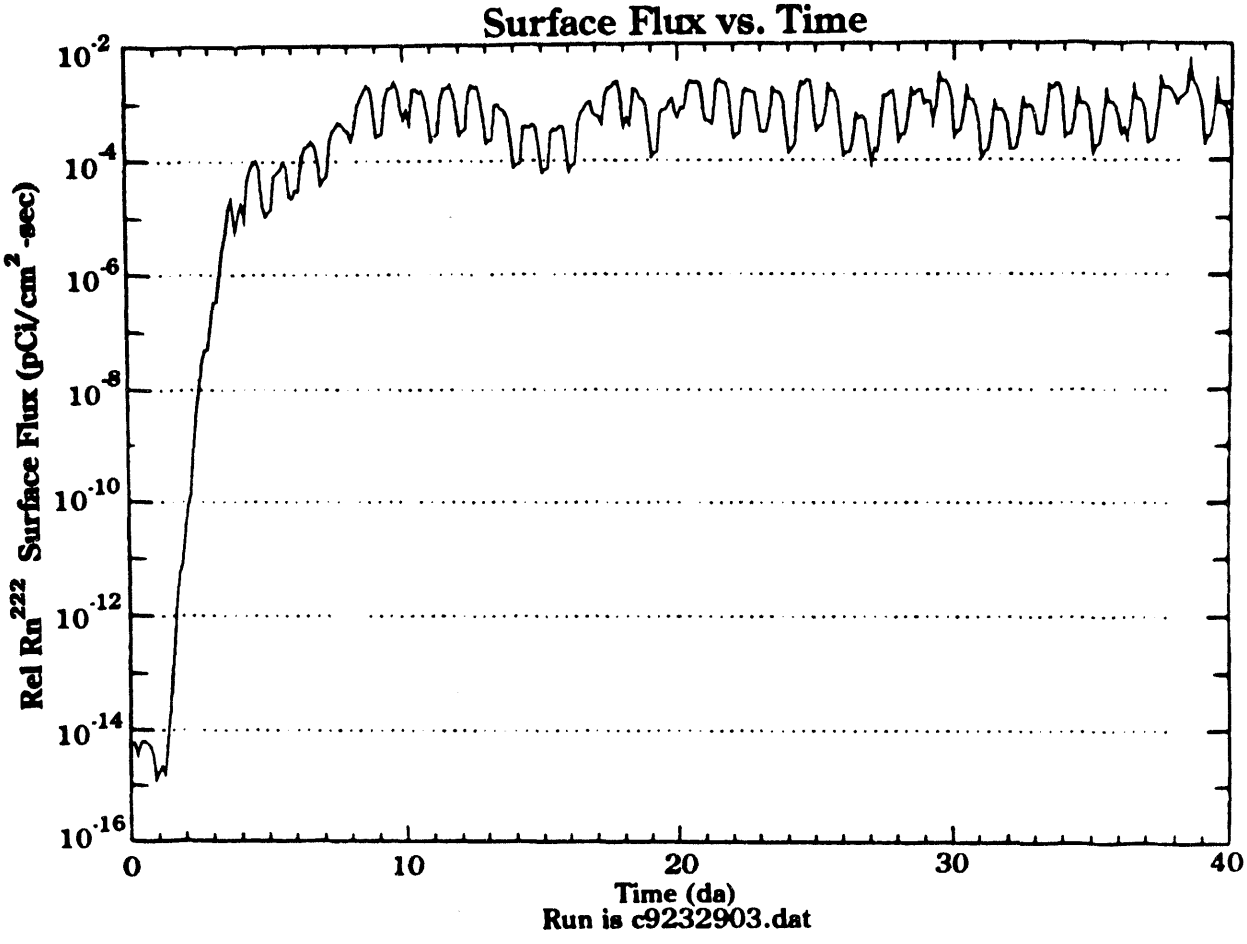

Figure 3.2.4 Alternative 2. Radon-222 surface flux (pCi/cm^2-sec).

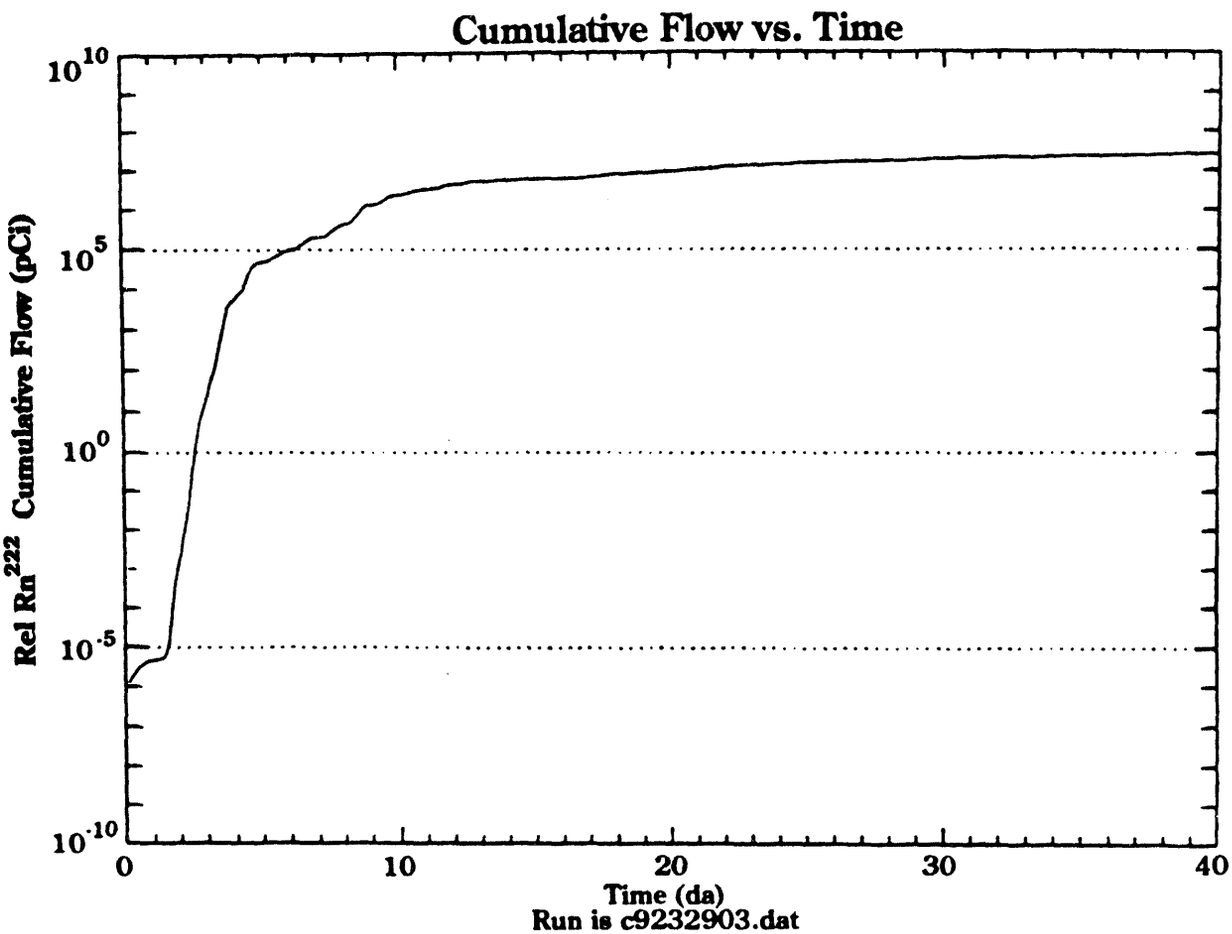

Figure 3.2.5 Alternative 2. Cumulative surface flow of radon-222 through 10^4 cm^2 of surface area (pCi).

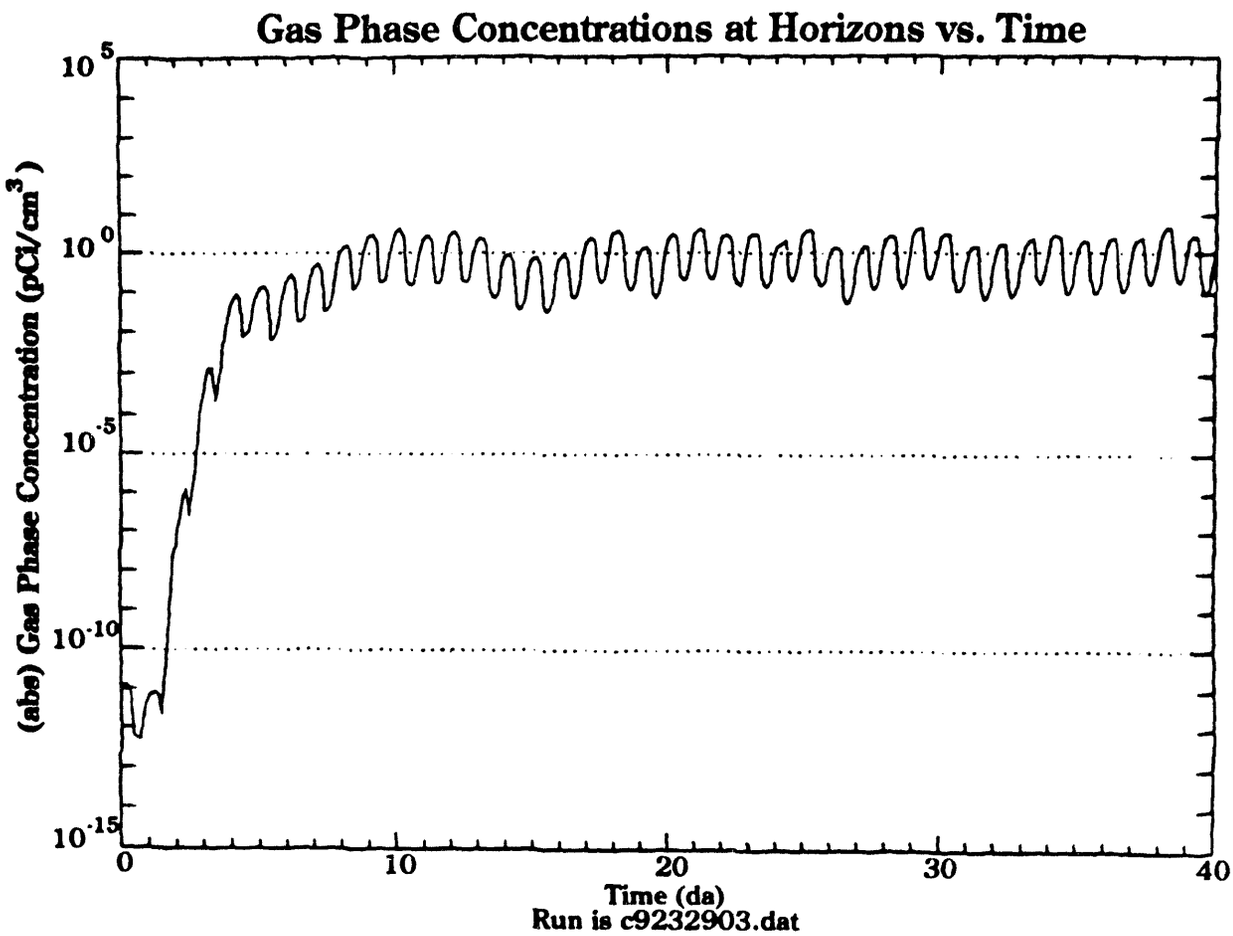

Figure 3.2.6 Alternative 2. Radon-222 gas-phase concentration (pCi/cm^3) at the alluvium-atmosphere interface.

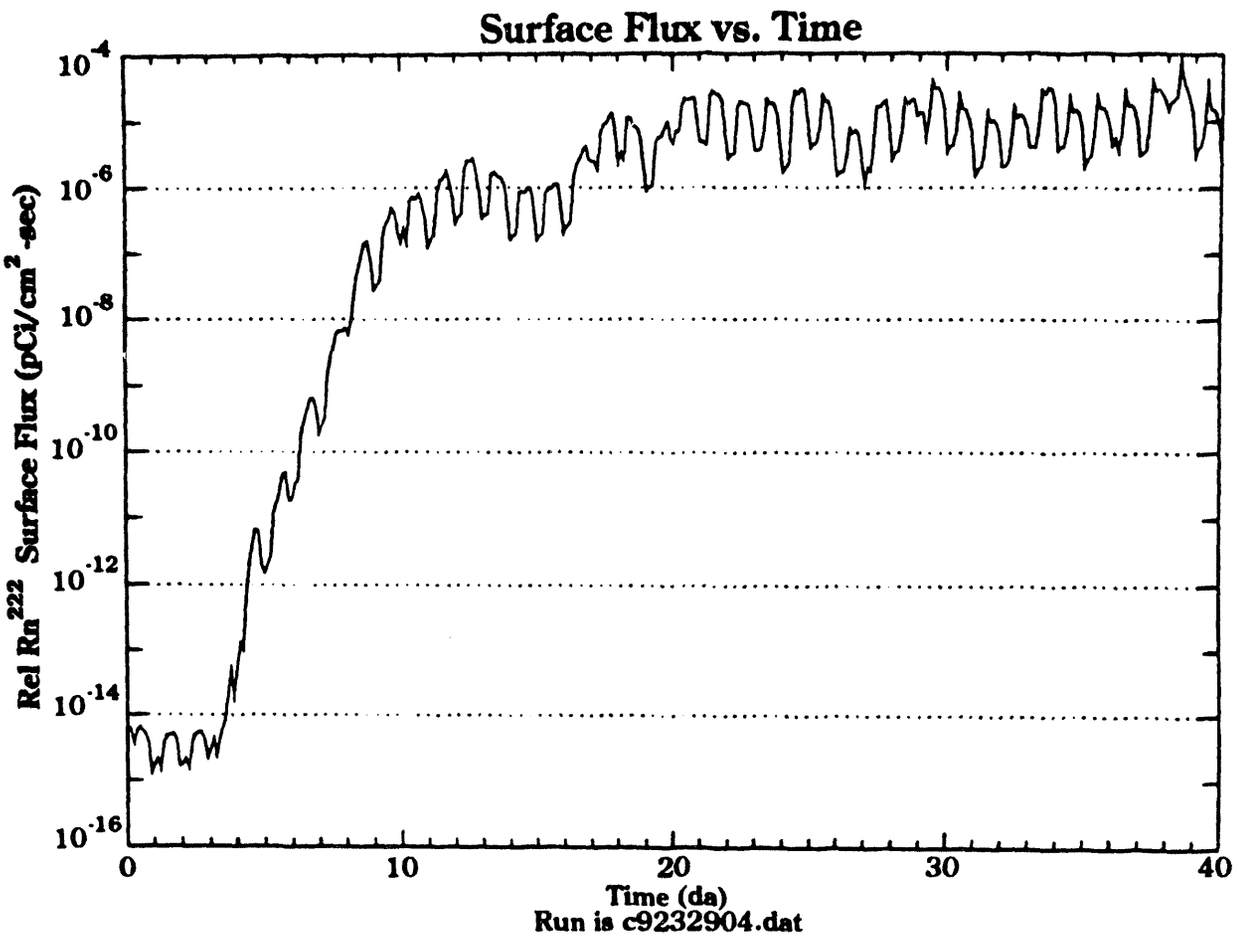

Figure 3.2.7 Alternative 3. Radon-222 surface flux (pCi/cm^2-sec).

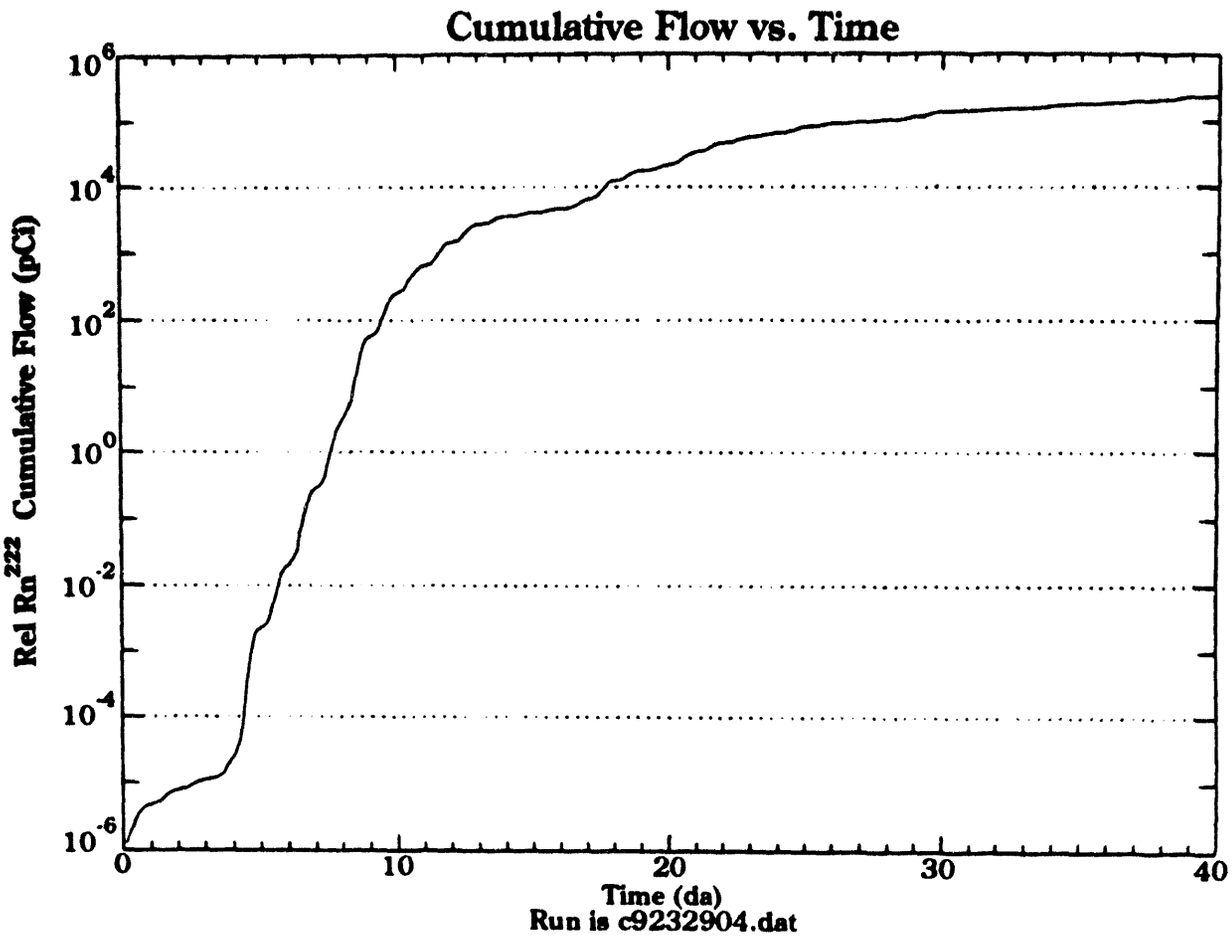

Figure 3.2.8 Alternative 3. Cumulative surface flow of radon-222 through 10^4 cm^2 of surface area (pCi).

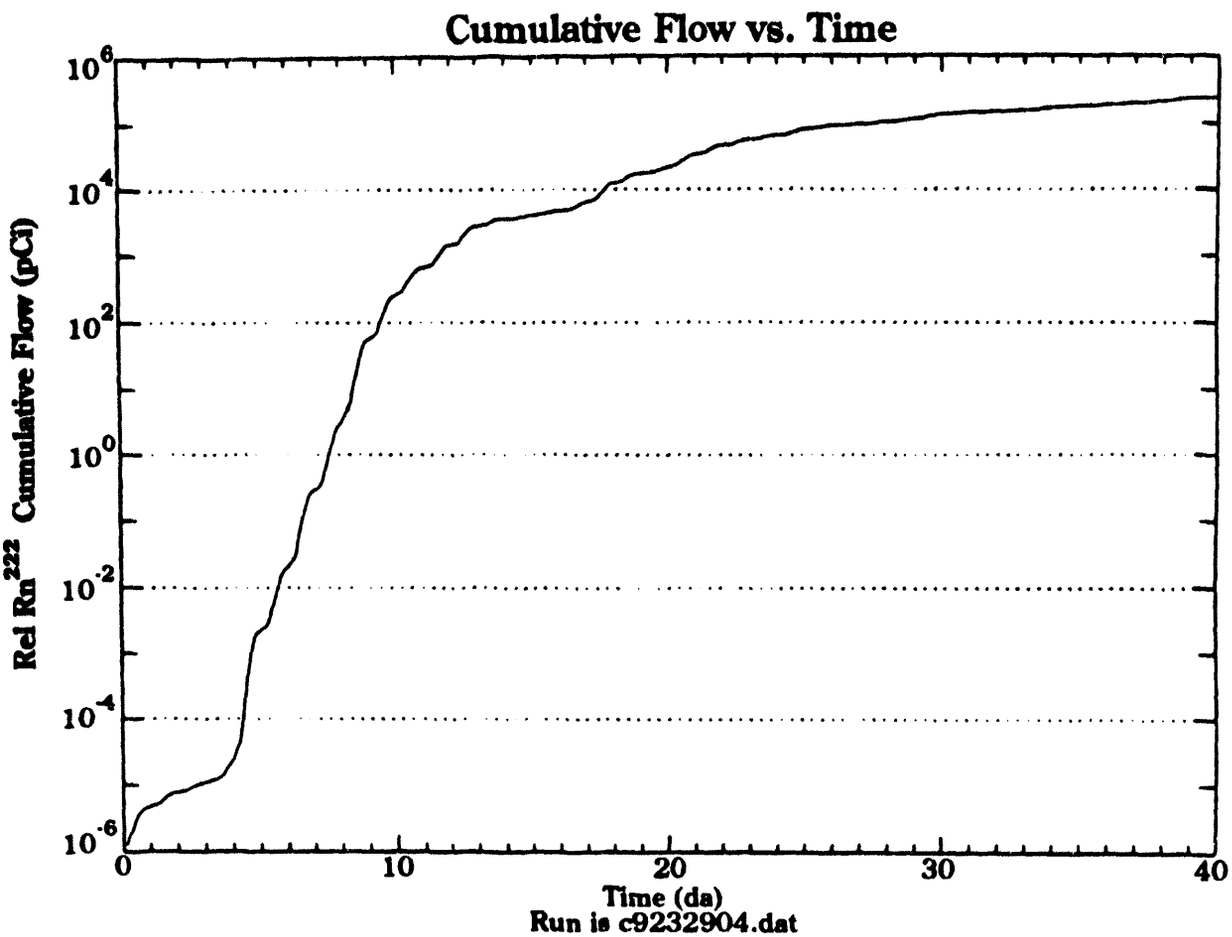

Figure 3.2.9 Alternative 3. Radon-222 gas-phase concentration (pCi/cm^3) at the alluvium-atmosphere interface.

this section indicate. Figure 3.2.7 (the radon-222 surface flux) clearly shows that the peaks in radon-222 flux are now well below an order of magnitude below the NESHAP standard. Observe the progressive lag in the time to steady-state in the radon-222 surface flux as burial depth is increased. At this depth it takes about 20 days to come to steady-state flux. No engineered cap is used, only the 11.2 meters of native soil as a backfill material over the top of the waste region. The same 40-day barometric pressure data, as discussed before, was used.

Alternative 4 (X_T = 1,420 cm, X_B = 1,520 cm)

In this scenario the single tier source top is placed at 1,420 cm below grade while the bottom of the source is placed 1,520 cm below grade. Figures 3.2.10 through 3.2.12 summarize the same attributes of CASCADR8 as the figures for the first three alternatives do. The radon-222 surface flux time distribution, shown in Figure 3.2.10 comes into steady-state about day 35. The peak in the radon-222 surface flux lies at least two orders of magnitude below the NESHAP standard. Figure 3.2.11 shows the time cumulative radon-222 flow through 10^4 cm^2 of surface, while Figure 3.2.12 shows the radon-222 gas-phase concentration (pCi/cm^3) at the alluvium-atmosphere interface. The same 40-day barometric pressure data was used in generating these attributes over time.

Alternative 5 (X_T = 2,840 cm, X_B = 2,940 cm)

In this scenario the single tier source top is placed at 2,840 cm below grade while the bottom of the source is placed 2,940 cm below grade. This case can be considered deep burial, since a burial depth of 2,840 cm is essentially 93.1 feet below grade. The same 40-day barometric pressure data was used as per the proceeding four alternatives. The time distribution of radon-222 surface flux is shown in Figure 3.2.13. The levels are at least ten orders of magnitude under NESHAP. However, the radon-222 surface flux has not come into a steady-state by day 40. Therefore, a 400-day run, starting with a repeat of the first 40 days of real barometric pressure

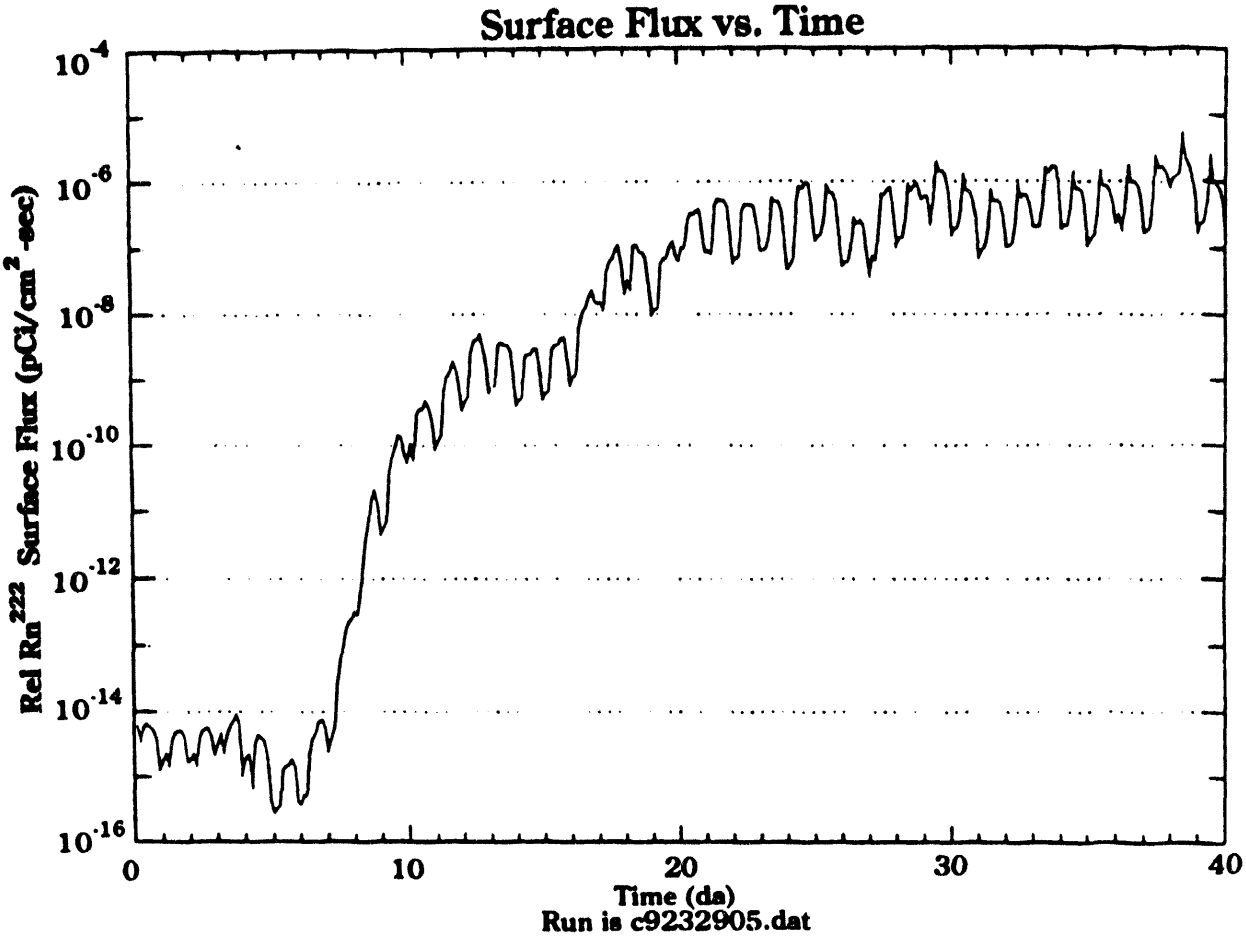

Figure 3.2.10 Alternative 4. Radon-222 surface flux (pCi/cm^2-sec).

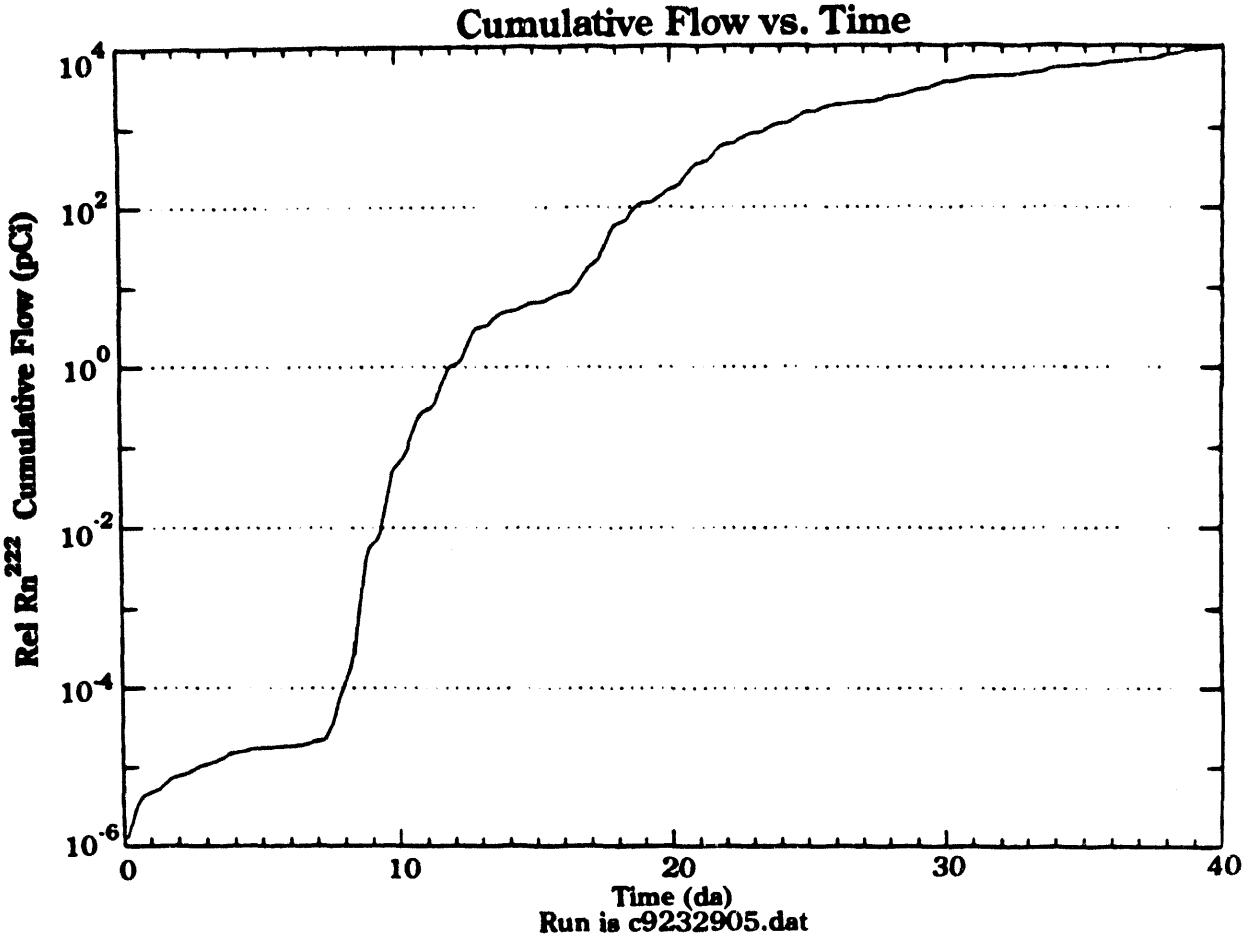

Figure 3.2.11 Alternative 4. Cumulative surface flow of radon-222 through 10^4 cm^2 of surface area (pCi).

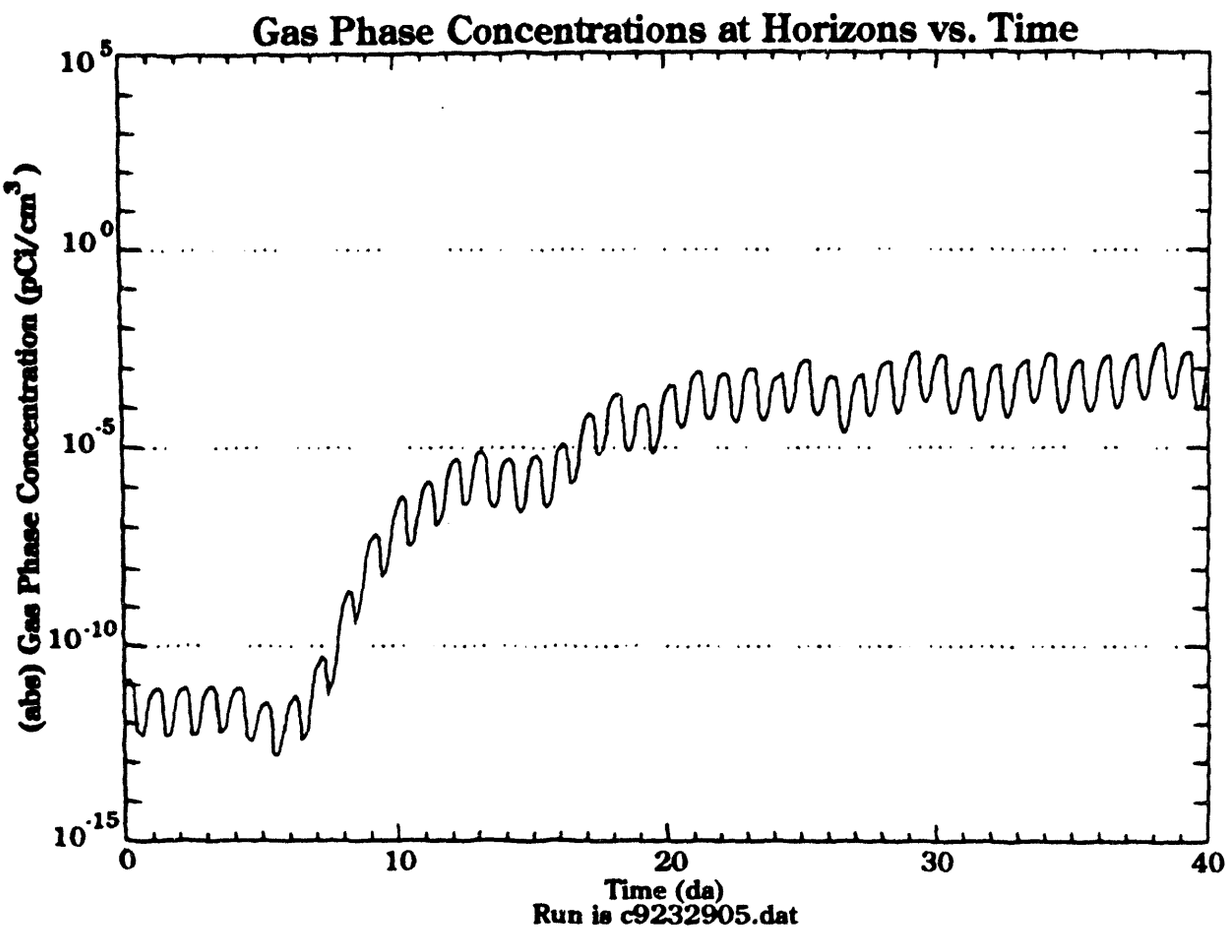

Figure 3.2.12 Alternative 4. Radon-222 gas-phase concentration (pCi/cm^3) at the alluvium-atmosphere interface.

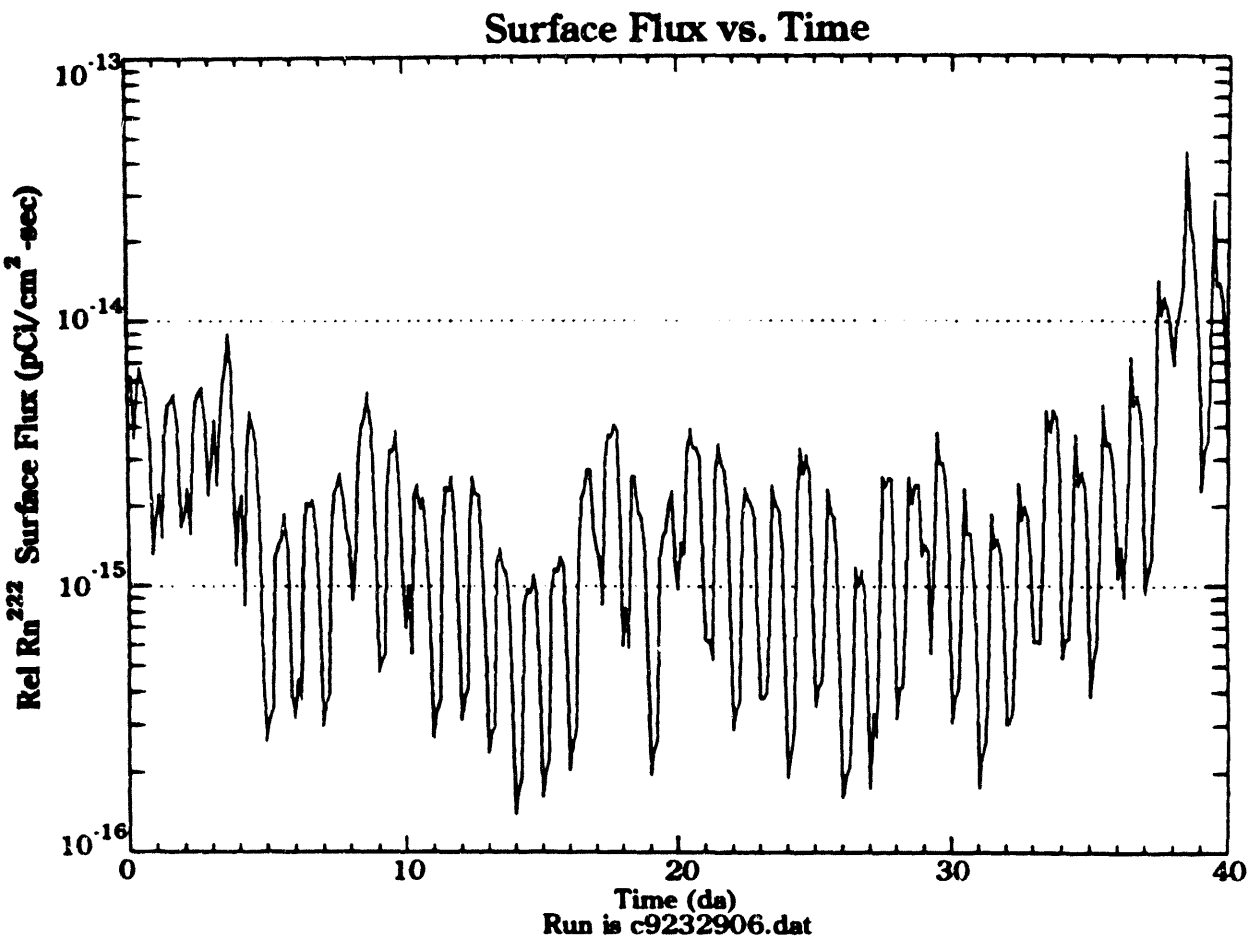

Figure 3.2.13 Alternative 5. Radon-222 surface flux (pCi/cm^2-sec).

data, followed by the next 360 days of actual Lagrange cubic spline interpolated real barometric pressure data, was made. The surface flux of radon-222 for the 400-day run is shown in Figure 3.2.14. Clearly, the radon-222 surface flux comes into a steady-state about day 60. The peak flux is about eight orders of magnitude below the NESHAP standard. The additional long period changes in the flux are likely due to the combined seasonal and semi-annual barometric pressure effects as shown in Figure 3.2.15. Figure 3.2.16 shows the cumulative radon-222 flows off a surface area of 10^4 cm^2 at the alluvium-atmosphere interface. Since the steady-state flux had not been reached by 40 days, Figure 3.2.17 shows the same cumulative flow distribution only now plotted for the 400-day run. Figure 3.2.18 shows the radon-222 gas-phase concentration distribution at the surface over time for the 40-day simulation run. Figure 3.2.19 shows the same thing except the simulated concentration data is from the 400-day run.

3.3 Depth of Burial Effect on Surface Flux

In Appendix F of Cawlfield et al. (1992) formulas are developed that allow the estimation of the surface flux of radon-222, in the case of a homogeneous, isothermal, very dry porous medium, for purely diffusional transport and simple first order decay processes. The formulas give simple exponential dependencies, especially for long times, i.e., steady-state of the surface flux on 1) depth of burial and 2) the source region thickness. The simulations conducted here are not strictly diffusional. The valving action of the boundary layer effective gas transfer diffusivity together with barometric air pressure induced advective pumping combine to produce not negligible real effects. Therefore, it is unknown at this time just how applicable the exponential fall off of surface flux might be by increasing the depth of burial. However, in the spirit of an engineering design study, the daily mean surface flux for the 40th day have been plotted on semi-log paper as a function of the depth to the center of the waste region in Figure 3.3.1. The dotted line is the regression line obtained using the 40-day daily mean surface fluxes for alternative one through four. The 400-day daily mean surface flux for alternative five is used as the fifth data point in the regression.

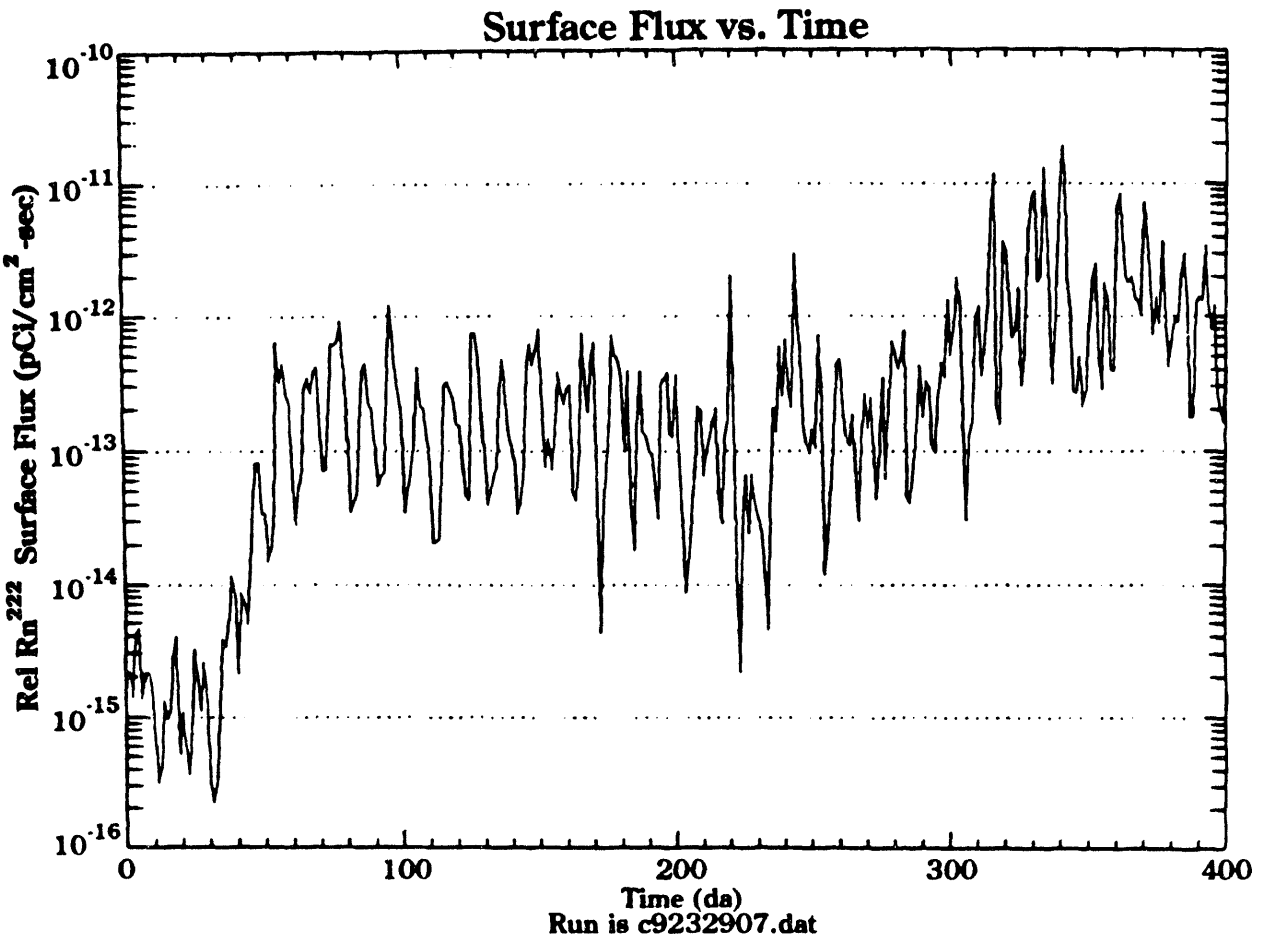

Figure 3.2.14 Alternative 5. Radon-222 surface flux (pCi/cm^2-sec) 400 day simulation.

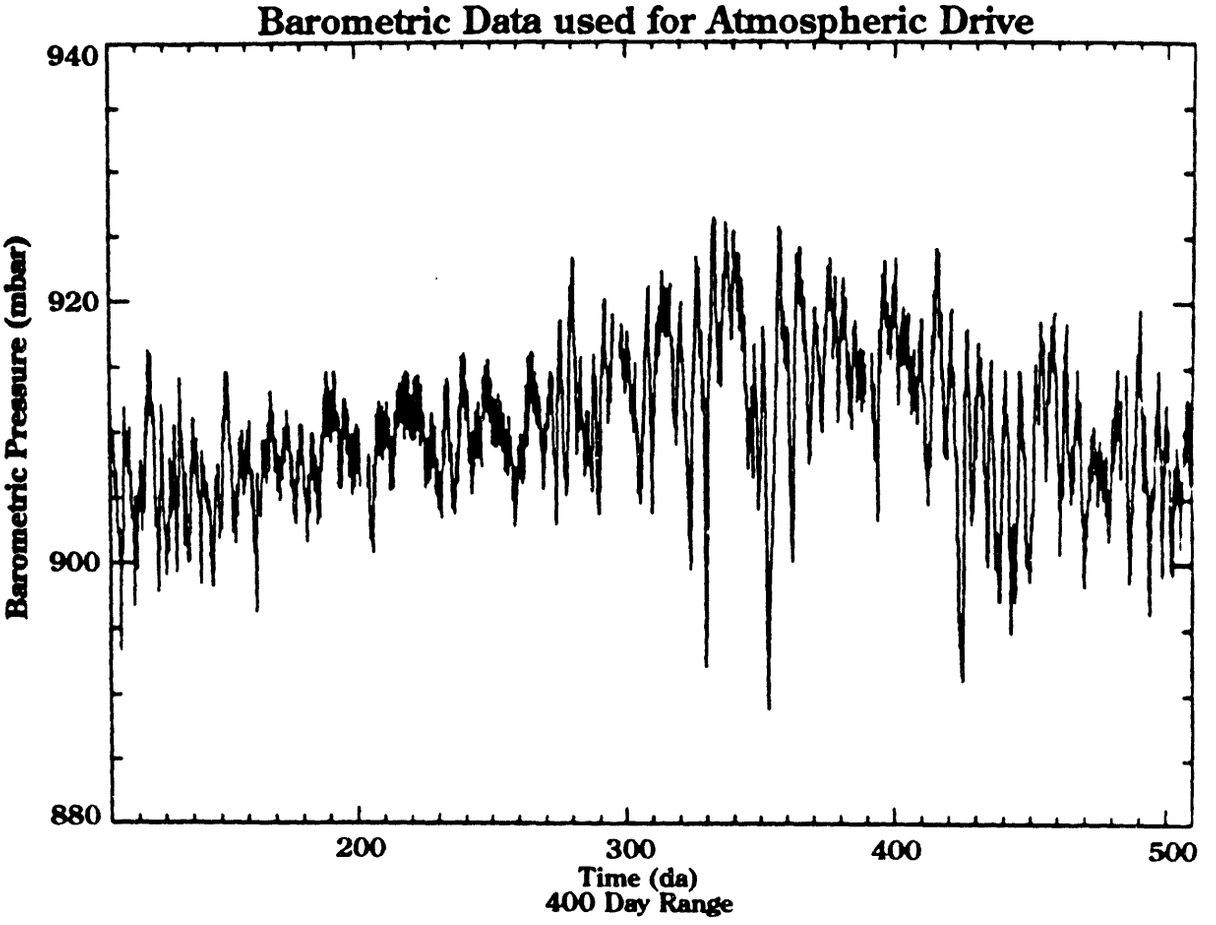

Figure 3.2.15 Alternative 5. Barometric pressure data (mb) over the 400 days simulation time.

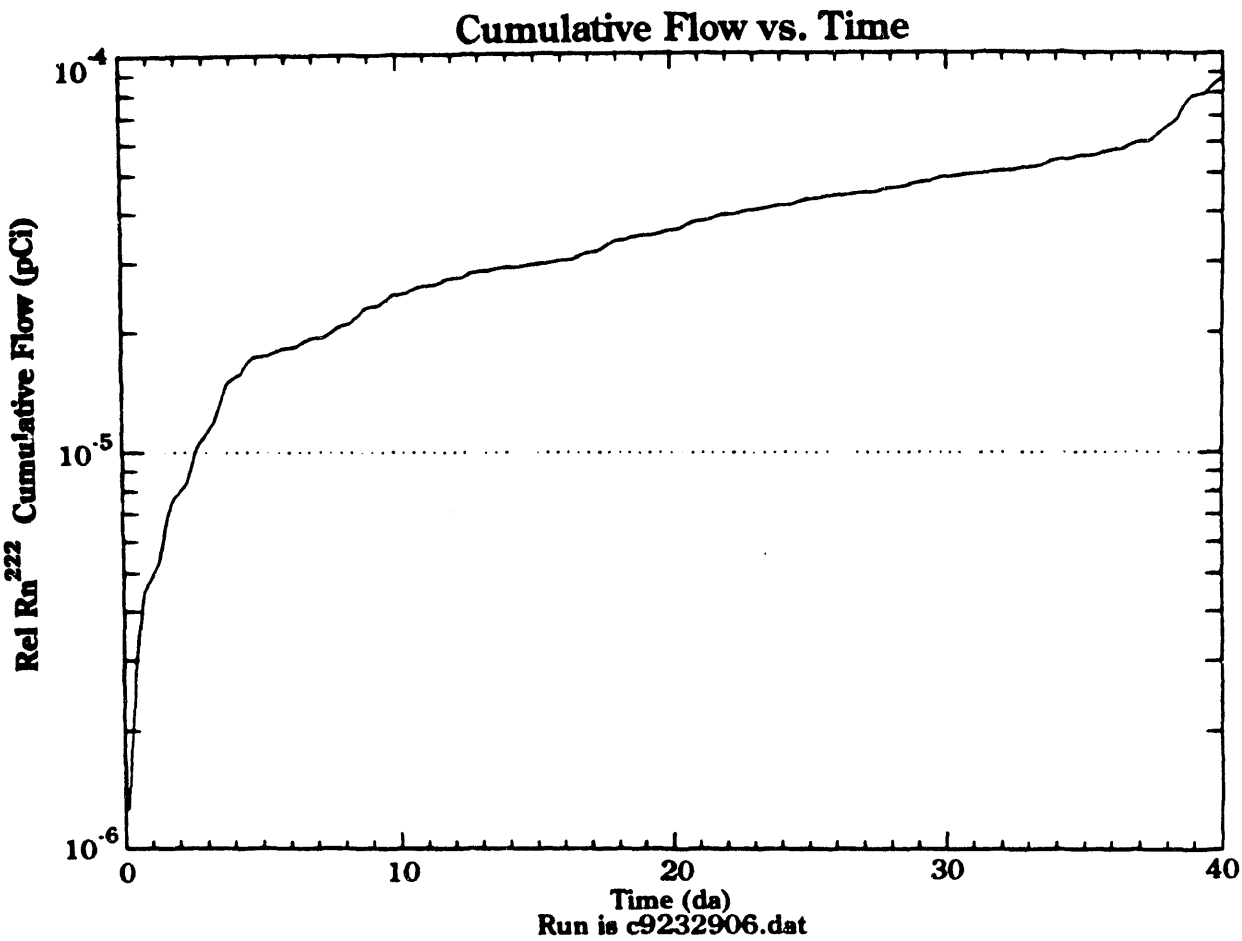

Figure 3.2.16 Alternative 5. Cumulative surface flow of radon-222 through 10^4 cm^2 of surface area (pCi).

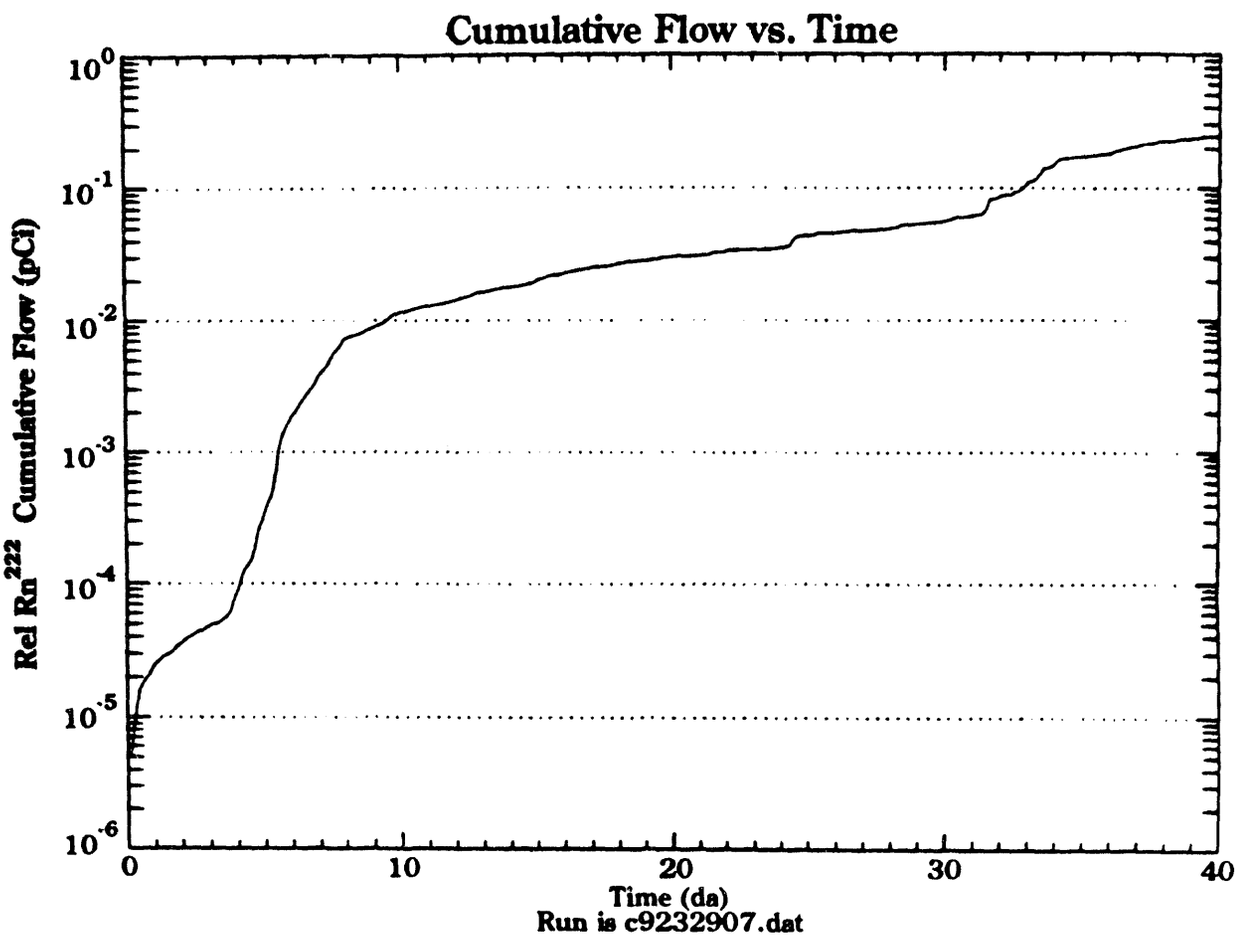

Figure 3.2.17 Alternative 5. Cumulative surface flow of radon-222 through 10^4 cm^2 surface area (pCi) 400 day simulation time.

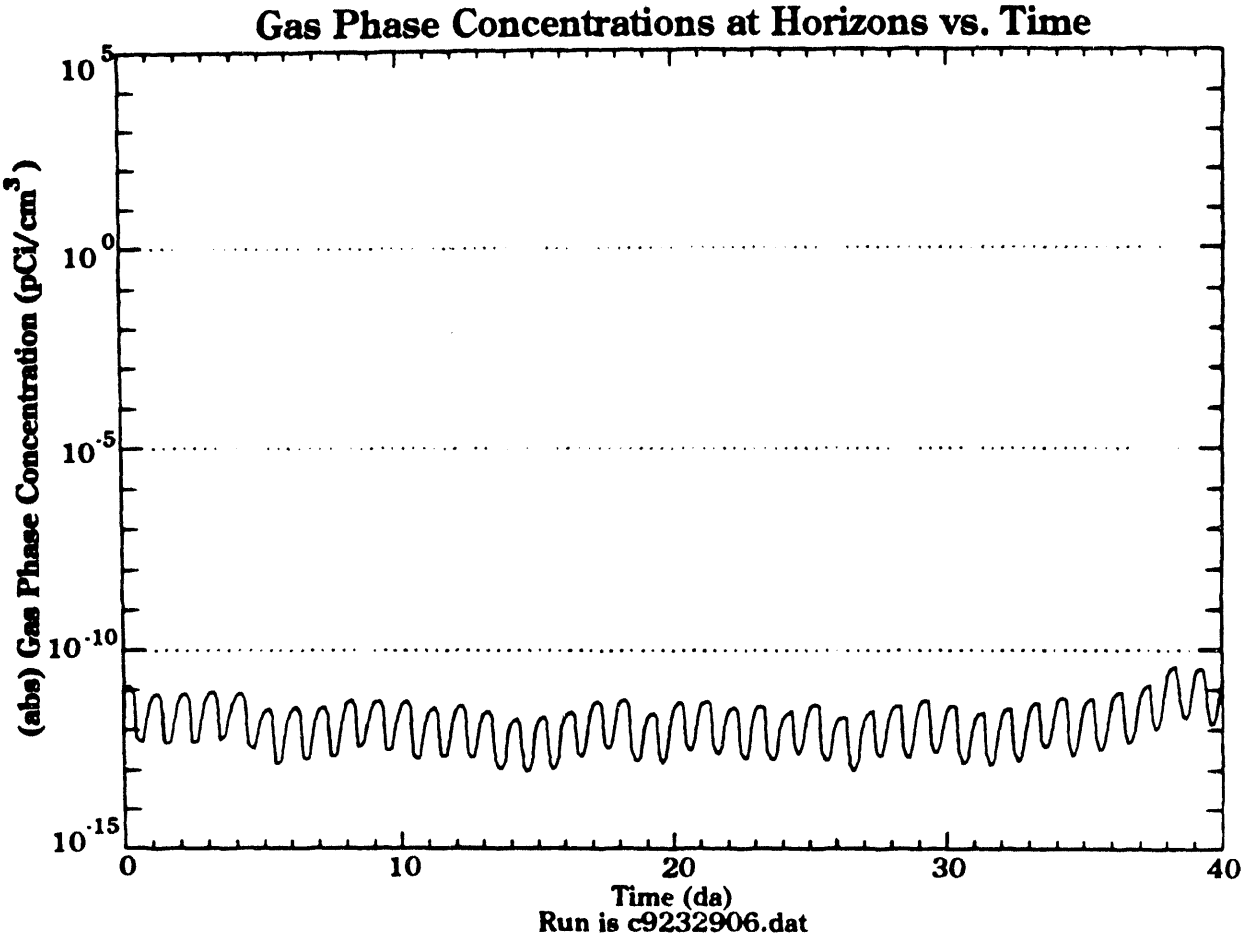

Figure 3.2.18 Alternative 5. Radon-222 gas-phase concentration (pCi/cm^3) at the alluvium-atmosphere interface.

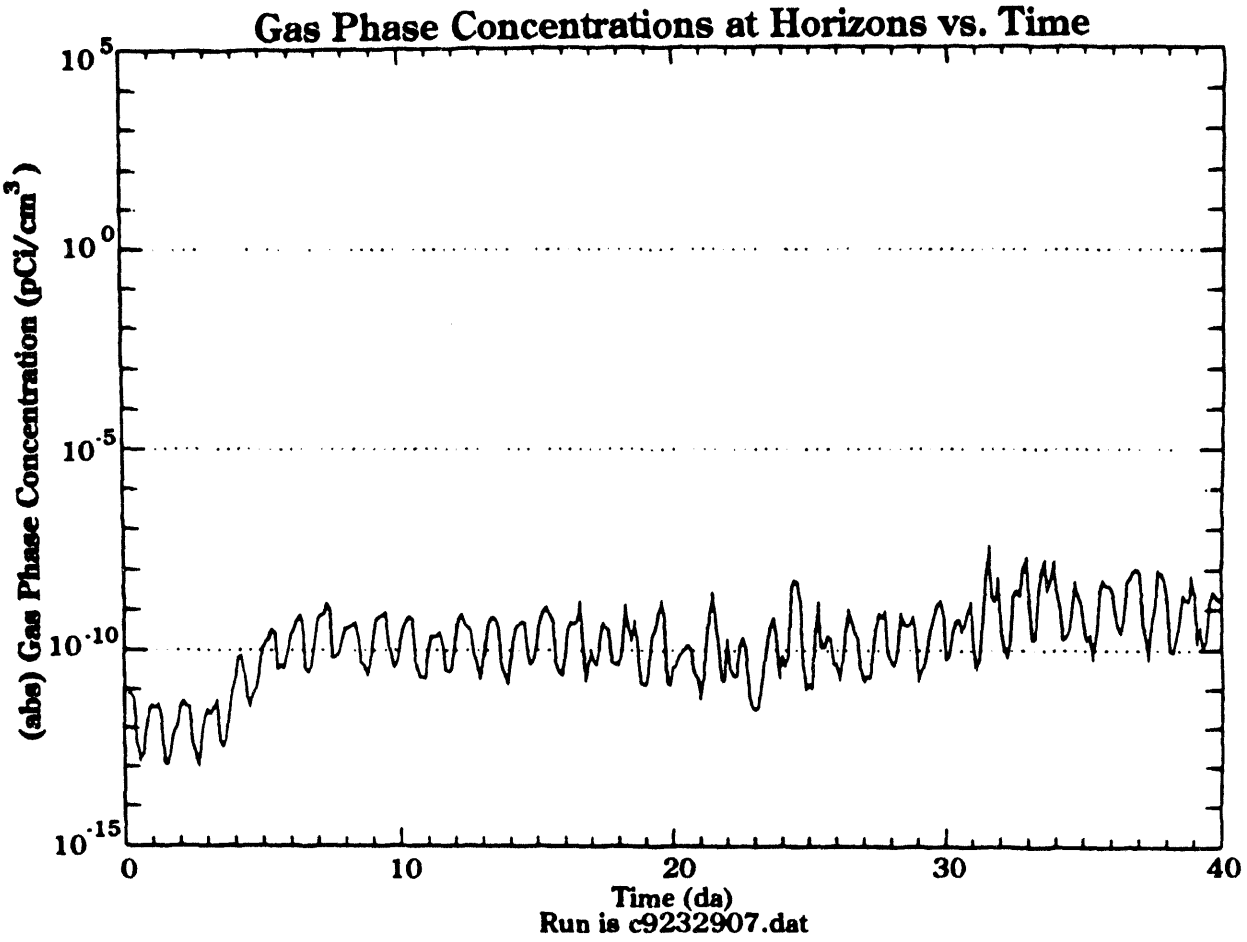

Figure 3.2.19 Alternative 5. Radon-222 gas-phase concentration (pCi/cm^3) at the alluvium-atmosphere interface. 400-day run.

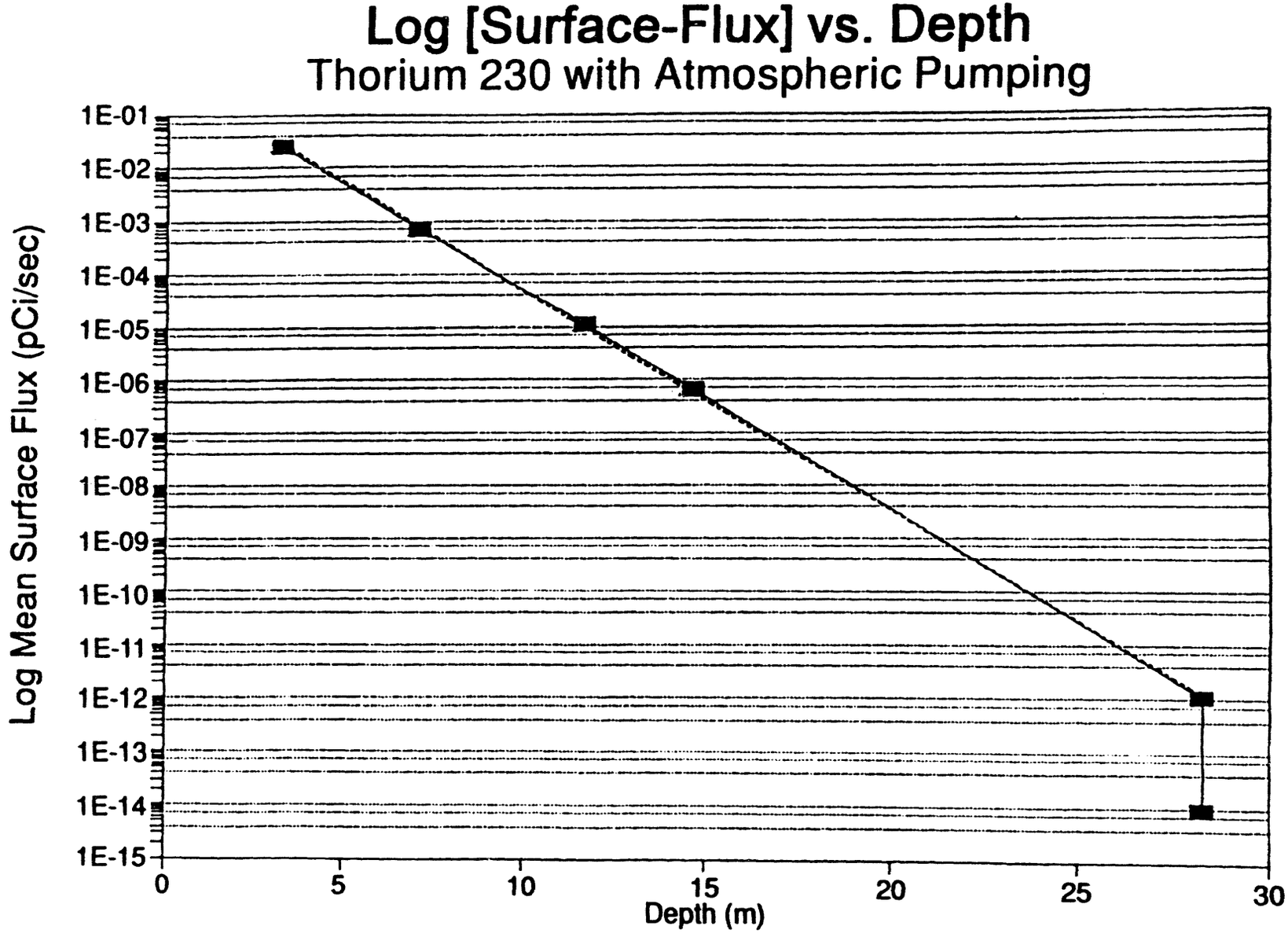

Figure 3.3.1 Daily mean flux on day 40 vs. mean burial depth.

The lower data point, at mean depth 28.3 meters, is the daily mean flux valve obtained for day 40 under alternative five conditions. Table 3.3.1 shows the raw data, the log transformed data, and the two sets of regressions. Clearly, using the data point at 40 days and alternative five conditions (flux is not at steady-state yet) causes an inferior regression. Despite the fact that the surface has a time dependent valving action operating as well as the time dependent induced advection, the semi-log plot yields a surprisingly good straight line, which implies that surface flux is dependent exponentially upon the mean burial depth. The nonlinear effect of the source thickness, predicted in Appendix F of Cawlfield et al. (1992) can not be assessed here since all the alternatives were run with a constant one meter thick source region.

Table 3.3.1 Quattro Pro 3.1 Regression Statistics for Daily Mean Flux pCi/cm^2-sec

Thorium 230 with Atmospheric Pumping 1 m layering					
	Run	Mean Depth (m)	Rate (pCi/cm^2-sec)	Ln (Rate)	Fit (5)
	C9232902	3.3	2.356E-02	-3.748E+00	2.756E-02
	C9232903	7.1	6.787E-04	-7.295E+00	7.339E-04
	C9232904	11.7	1.075E-05	-1.144E+01	9.109E-06
	C9232905	14.7	6.407E-07	-1.426E+01	5.204E-07
400-day	C9232907	28.3	1.049E-12	-2.758E+01	1.204E-12
40-day	C9232906	28.3	9.434E-15	-3.229E+01	1.204E-12
Regression Output: All Six Points					
Constant			0.45899		
Std Err of Y Est			1.79825		
R Squared			0.98008		
No. of Observations			6.00000		
Degrees of Freedom			4.00000		
X Coefficient(s)			-1.06399		
Std Err of Coef.			0.07585		
Regression Output: First Five Points					
Constant			-4.427E-01		
Std Err of Y Est			2.004E-01		
R Squared			9.996E-01		
No. of Observations			5.000E+00		
Degrees of Freedom			3.000E+00		
X Coefficient(s)			-9.541E-01		
Std Err of Coef.			1.045E-02		

4.0 ASSESSMENT OF DOSES FROM PROJECTED RADON-222 EMISSIONS

4.1 Regulatory Requirements

The purpose of this radiological assessment is to select a disposal option for purified thorium waste that meets all applicable regulations. This assessment considers only inhalation doses from radon-222 progeny generated from the serial radioactive decay of thorium-230.

Waste disposal at DOE facilities is governed by DOE Order 5820.2A, Radioactive Waste Management. This order requires that releases to the atmosphere meet the requirements of Title 40 Code of Federal Regulations (CFR) Part 61, the National Emission Standard for Hazardous Air Pollutant. Subpart Q of (NESHAP), and the National Emission Standards for Radon Emissions from Department of Energy Facilities, states that no source at a DOE facility shall emit more than 20 $pCi/m^2/s$ (2×10^{-3} $pCi/cm^2/s$) of radon-222 as an average for the entire source. This standard applies to disposal facilities that manage byproduct material as defined under section 11.e(2) of the Atomic Energy Act. The thorium waste more closely meets the definition of source material as defined in section 11.z(1). Since there is no radon-222 emission standard for source material, it is assumed that at the time of disposal this waste stream can be considered 11.e(2) byproduct material and that 40 CFR 61, and Subpart Q of NESHAP apply. Much of the NESHAP deals with monitoring requirements. Obviously, compliance with monitoring requirements is impossible after the loss of institutional control. It is assumed that DOE Order 5820.2A requires selective application of the emission standard portion of 40 CFR 61 beyond the period of institutional control. Therefore, the period of compliance for the emission standard of the NESHAP is assumed to be 10,000 years.

In addition to the 40 CFR 61 requirements, DOE Order 5820.2A sets intruder committed effective dose equivalent (H_E) limits for continuous exposure. The requirement is that the H_E received by individuals who inadvertently intrude into the

facility after the loss of institutional control shall not exceed 100 mrem/yr. The period of compliance with this requirement is taken from 100 years to 10,000 years.

Since there are many potential intruder exposure pathways, it is desirable that exposure from radon-222 remain much less than the 100 mrem/yr limit. The objective of this analysis is to select a disposal option that yields predicted radon-222 fluxes less than 2×10^{-3} pCi/cm^2/s and an H_E that is a small fraction of 100 mrem/yr.

4.2 Radiological Assessment Model

Compliance with the NESHAP has been assessed by comparison of the standard with the radon-222 fluxes predicted by the CASCADR8 model for several waste disposal options. The results of these analyses are discussed in Section 3. Compliance with the intruder H_E limits was evaluated with a radiological assessment model described below. The intruder H_E limit was found to be the most restrictive.

The principal exposure pathway for an intruder was assumed to be inhalation of radon progeny in a structure built on a waste disposal cell. The primary source of radon in the structure was assumed to be radon transported from the soil-pore-gas to room air. Another potential entrance pathway is the release of radon from groundwater pumped into the structure. The groundwater pathway was not considered because the mean time required for radionuclides to leach through the vadose zone is estimated to be at least 20,000 years.

Appendix C presents the mathematical details of a model that predicts H_E for intruders residing in a building constructed directly over a waste disposal cell. The model is extremely conservative and is expected to significantly over estimate the dose equivalents possible. The model assumes the waste is pure thorium-230 at time zero and that radium-226 and radon-222 are formed by serial radioactive decay. It is assumed that leaching or erosion of the waste material does not occur. The concentration of radon-222 in soil pore gas at a depth of z=0 meters is assumed to be proportional to the activity concentration of radium-226 in the waste. This constant of

proportionality is derived from the CASCADR8 model and is based on the maximum soil-pore-gas concentrations predicted. The constant does not vary with changing atmospheric conditions and is specific for a given waste activity concentration, depth of burial and waste thickness. However, the radon-222 soil-pore-gas activity concentration will increase with time as radium-226 ingrowth occurs in the waste. The maximum H_E will occur at the time of maximum radium-226 concentration, which will occur approximately 9,100 years after separation.

Most houses in southern Nevada are constructed on concrete slabs. The entrance of radon into structures built on concrete slabs is dominated by advection of soil-pore-gas through penetration and cracks in the slab (Nazaroff 1992). For simplicity, soil-pore-gas was assumed to enter the house without dilution. It was concluded that parameterization of a model that considers dilution effects was not possible at this time. The assumption of no dilution is extremely conservative and probably predicts radon-222 concentrations several orders of magnitude above those likely to occur. Radon progeny are generated by radioactive decay of radon in room air. Radon progeny were assumed to be present at 0.4 of the equilibrium concentration (Appendix C).

Estimates of H_E are obtained by converting the concentration of polonium-218, lead-214, and bismuth-214 into potential alpha energy concentration (PAEC) in units of working levels and multiplying by the time of exposure and the H_E/working level month (WLM) conversion factor. Exposure was assumed to be continuous for a year and the intruders were assumed to spend 100% of their time on the site. The H_E/WLM conversion factor selected, 0.72 rem/WLM, was based on a dose equivalent conversion factor for the bronchial epithelium of 12 rem/WLM used in NCRP Report 94 (1987) and a weighting factor of 0.06 for the bronchial epithelium. The ICRP (1981) has reviewed two published radon lung dosimetry models and the ICRP 30 (1979) lung model. They set ranges for the H_E/WLM conversion factor that include the NCRP factor. The BEIR IV committee (NRC 1988) reviewed the same two published models and a third model and concluded that the models yield dose conversion factors that

are within a factor of three of each other. The BEIR IV committee further concluded that since these models cannot be validated by physical measurements, it is impossible to determine which model is the most accurate (NRC 1988). The ICRP has cautioned that dose conversion factors should be corrected for exposure conditions that differ from those assumed in the dosimetry model. The BEIR IV committee has attempted to develop a correction factor that considers the effects of particle size distribution, the unattached fraction, the equilibrium factor, and the breathing rate (NRC 1988). Their estimate of the ratio of H_E/WLM for residential exposures over H_E/WLM for mines was 0.94 (NRC 1988). Given the overall uncertainty of the lung dosimetry models, i.e., a factor of three, the correction factor for the exposure conditions has been assumed to be 1.0.

4.3 Results

Conservative estimates of committed effective dose equivalents have been made for intruders entering the site after loss of institutional control and occupying a structure built on a waste disposal cell. Six disposal alternatives have been investigated for a specific waste stream containing high purity thorium-232 with traces of thorium-230. In all cases the predicted H_E rises to a maximum around 9,100 years. The results have been summarized in Table 4.1.

Table 4.1. Summary of Intruder Committed Effective Dose Equivalents for Different Disposal Options

Disposal Option	Maximum radon-222 Soil Pore Gas Concentration at z=0 m from CASCADR8	k_s (m^3/l)	Maximum H_E (rem/yr at 9,100 yrs)
Tiers: 4 Depth of Burial: 2.8 m	2×10^5 pCi/l	2.9×10^{-5}	29,000
Tiers: 1 Depth of Burial: 2.8 m	1×10^5 pCi/l	1.4×10^{-5}	14,000
Tiers: 1 Depth of Burial: 6.6 m	6×10^3 pCi/l	8.7×10^{-7}	873
Tiers: 1 Depth of Burial: 11.2 m	100 pCi/l	1.4×10^{-8}	14
Tiers: 1 Depth of Burial: 14.2 m	8 pCi/l	1.1×10^{-9}	1.1
Tiers: 1 Depth of Burial: 28.4 m	3×10^{-5} pCi/l	4.3×10^{-15}	4.3×10^{-6}

The first disposal alternative (base case), four tiers of waste packages buried at approximately 2.8 meters, represents the current waste management practices at the Area 5 Radioactive Waste Management Site. The H_E over time is plotted in Figures 4.3.1 through 4.3.5. The H_E at the end of institutional control, 100 years, was estimated to be 1×10^3 rem/yr and rose to a maximum of 3×10^4 rem/yr. The assessment results for the first three disposal alternatives are plotted in Figures 4.3.1 through 4.3.3. In all three cases the predicted intruder H_E exceeds the limit at the end of institutional control. The fourth disposal option (Figure 4.4.4), one tier buried at 14.2 meters does not exceed the limit at 100 years, but eventually rises to a maximum of 1 rem/year. The fifth alternate met all the performance objectives. In order to determine an acceptable burial option, the relationship between depth of burial and the maximum H_E was investigated. From Figure 4.3.6 it can be seen that a burial of a single tier of thorium waste at approximately 16 meters to 17 meters is estimated to result in a H_E to an intruder of approximately 100 mrem/yr. The addition of three meters of soil reduces the H_E to approximately 10 mrem/yr. Since the committed effective dose equivalent limits are for the sum of all pathways, burial at a depth greater than 18 meters is recommended to allow for doses from other pathways.

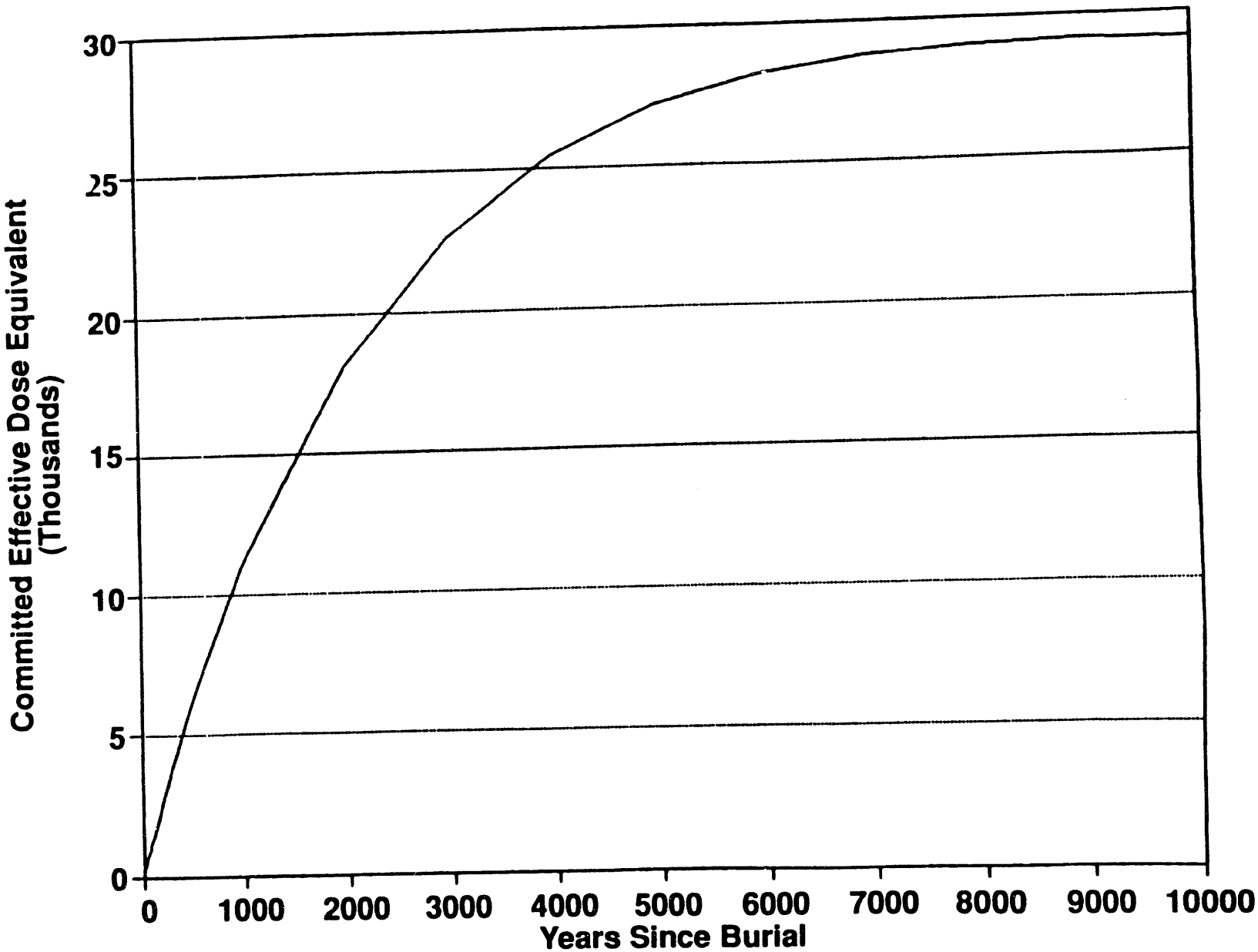

Figure 4.3.1 Intruder committed effective dose equivalent from inhalation of radon progeny; base case, burial of four tiers at 2.8 meters.

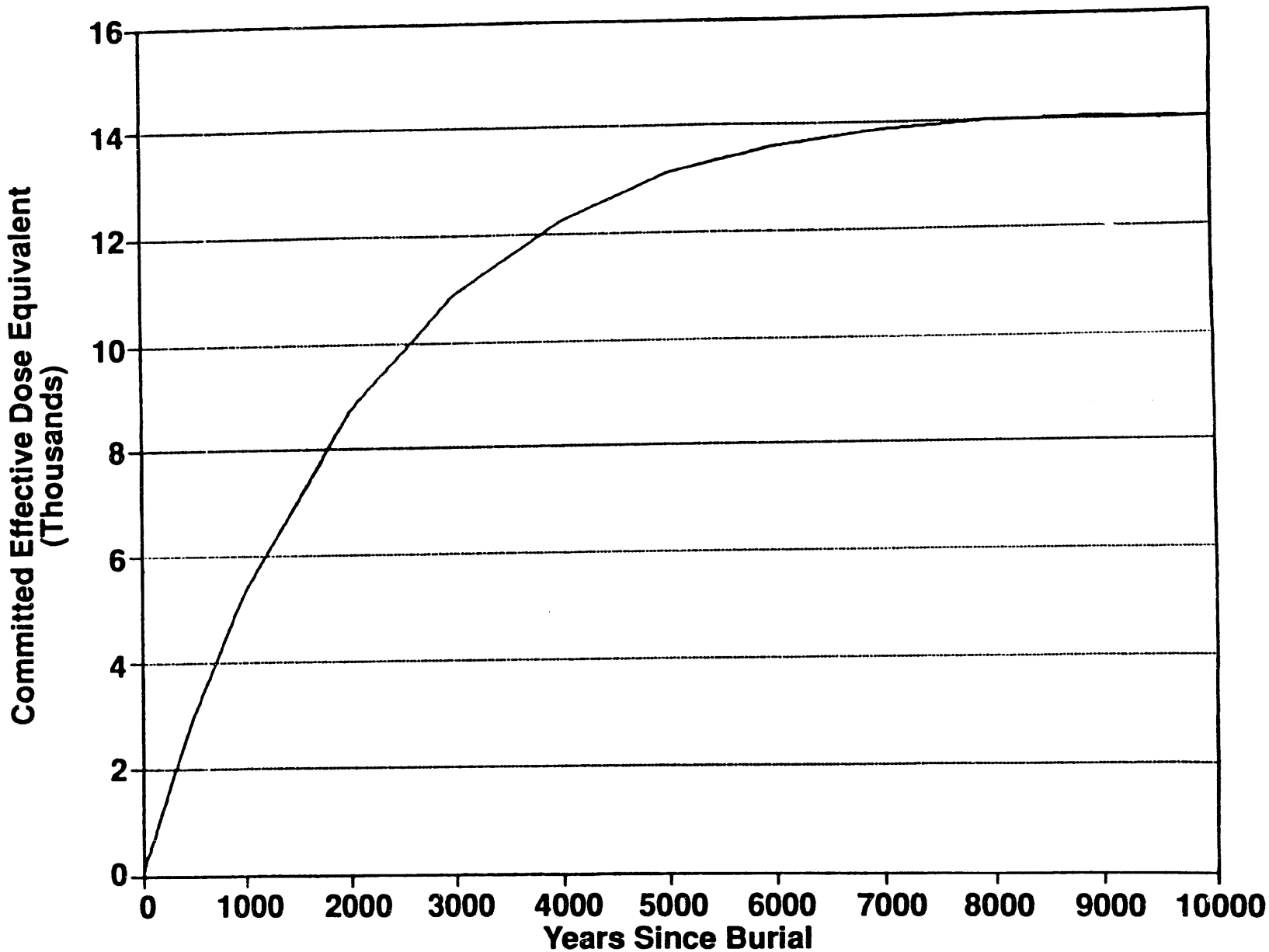

Figure 4.3.2 Intruder committed effective dose equivalent from inhalation of radon progeny; alternative 1, burial of one tier at 2.8 meters.

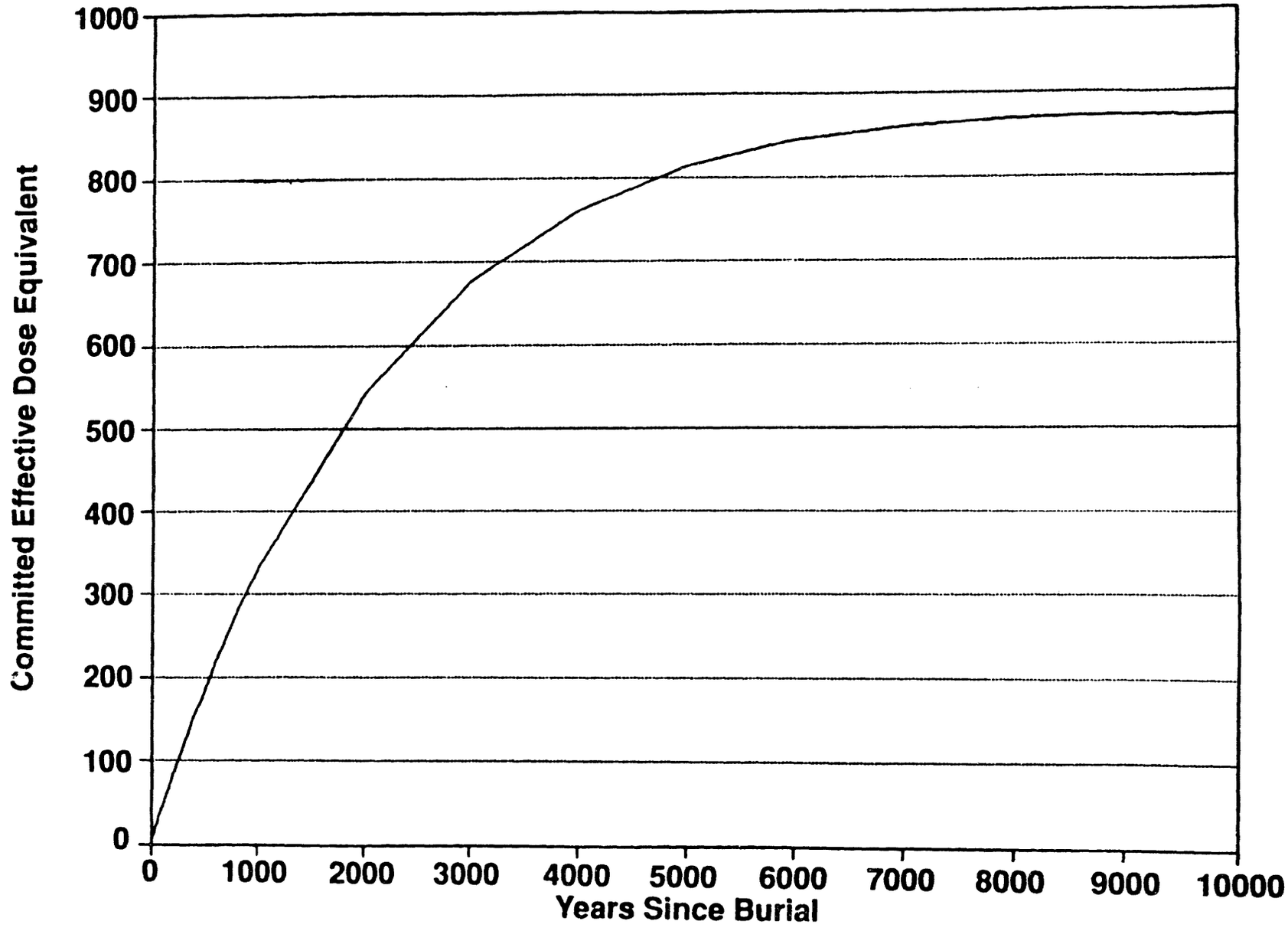

Figure 4.3.3 Intruder committed effective dose equivalent from inhalation of radon progeny; alternative 2, burial of one tier at 6.6 meters.

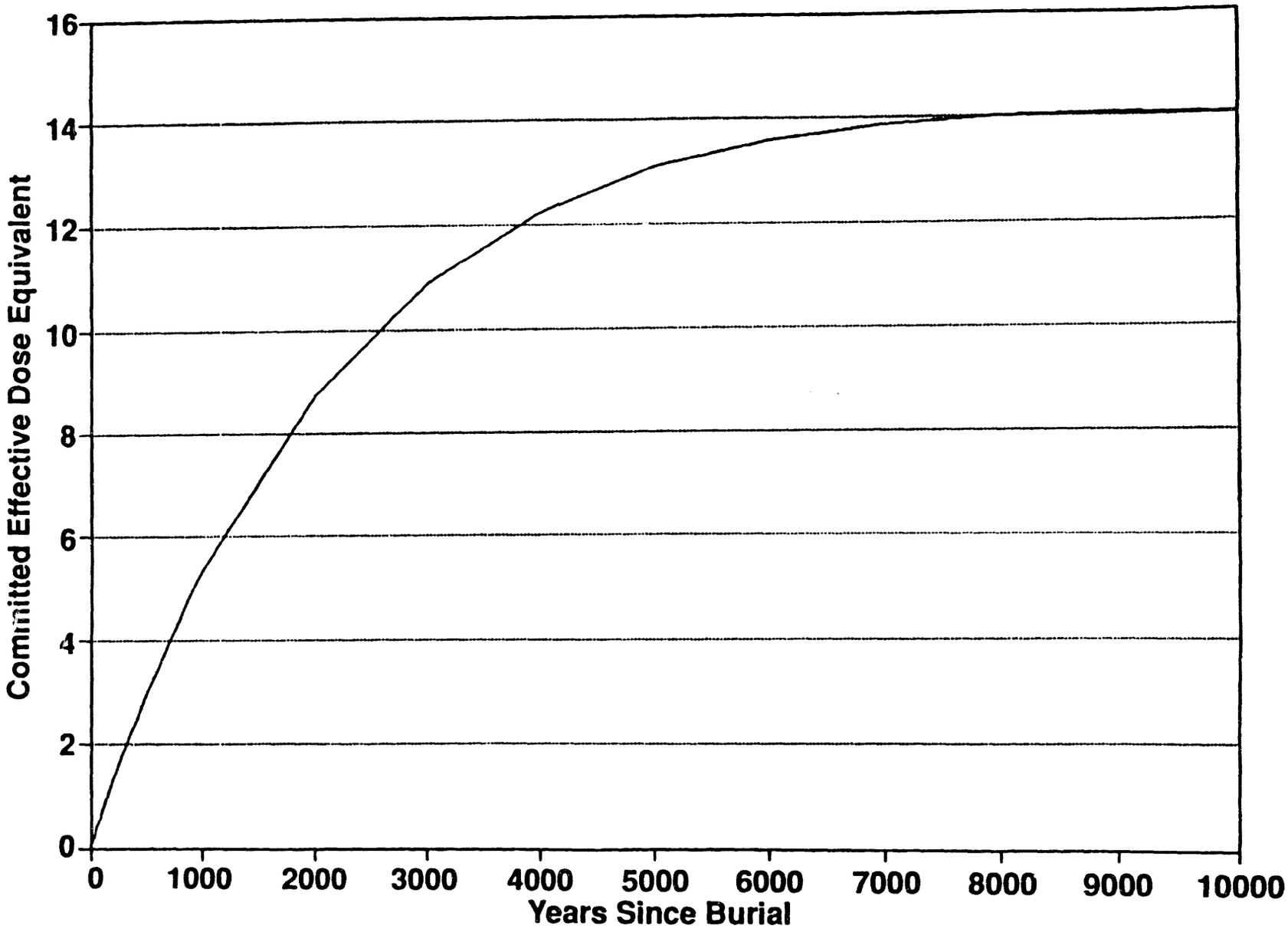

Figure 4.3.4 Intruder committed effective dose equivalent from inhalation of radon progeny; alternative 3, burial of one tier at 11.2 meters.

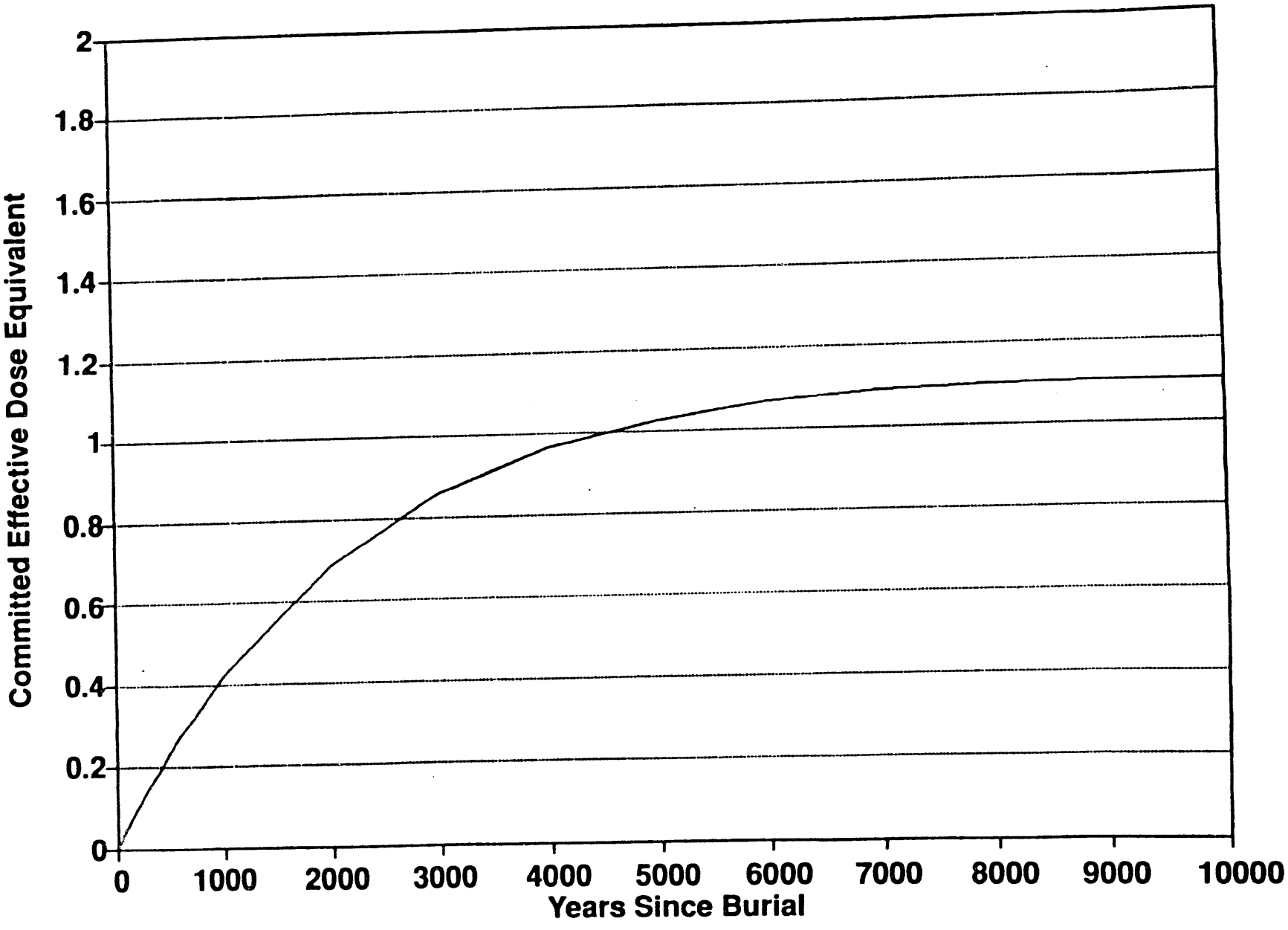

Figure 4.3.5 Intruder committed effective dose equivalent from inhalation of radon progeny; alternative 4, burial of one tier at 14.2 meters.

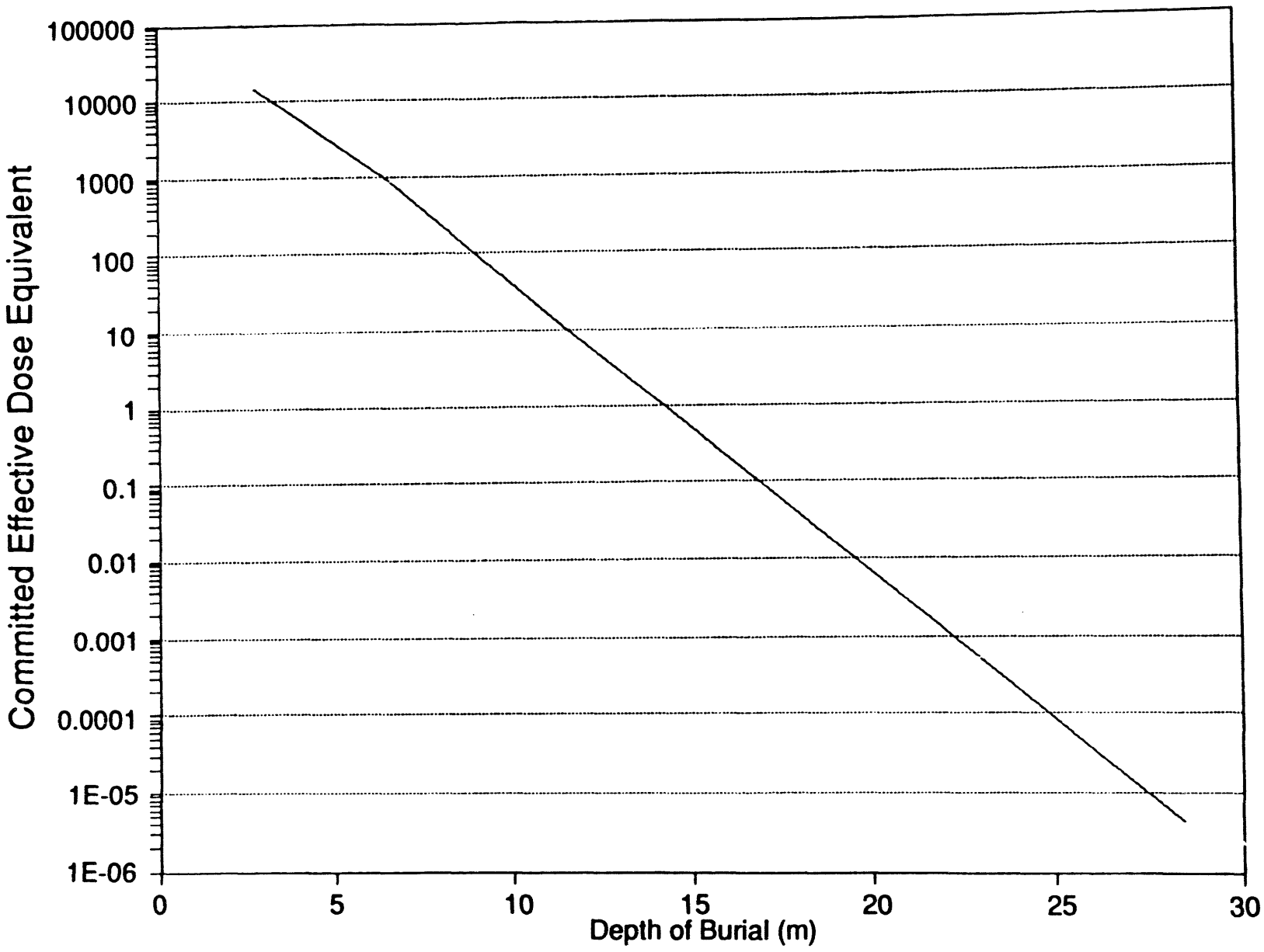

Figure 4.3.6 Intruder committed effective dose equivalent from inhalation of radon progeny versus depth of burial of a single tier of waste.

APPENDIX A

NOMENCLATURE

Several equations appear in the text. The mathematical symbols appearing in these equations are defined below in their order of appearance.

Symbol	Meaning	Units
$S_{sp}(z)$	radium-226 source rate function (assumed to be uniformly operating throughout the waste region)	gm/cm^3-sec
$C_{um}(t)$	cumulative radon-222 flow through area A (cm^2) at the soil-atmosphere interface	gm
$q\Big\|_{z=0} \cdot \hat{n}$	normal component of radon-222 flux at the soil-atmosphere interface	gm/cm^2-sec
A	characteristic cross-sectional area of soil-atmosphere interface	cm^2
t	elapse time from commencement of radon-222 release	sec
z	depth below soil-atmosphere interface	cm

APPENDIX B

CHEMICAL MASS FORM OF BATEMAN CASCADE RADIONUCLIDE CHAIN

The chemical mass form of the Bateman cascade chain is shown in the sketch below.

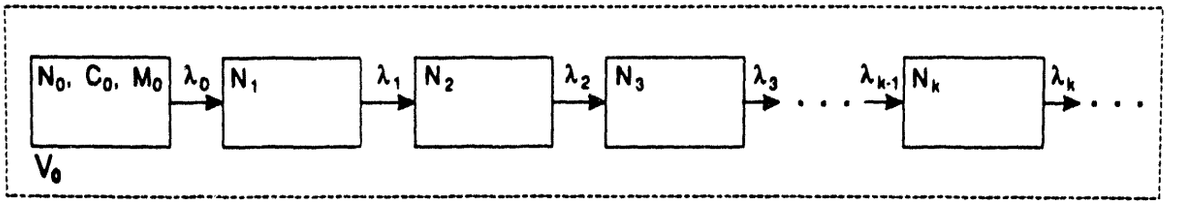

Figure B.1 Bateman Cascade Chain

Let N_0 be the number of atoms of radionuclide zero (parent) in the first "compartment." The volume of the space containing these atoms is V_0 (cm^3).
Let M_0 be the atomic weight of radionuclide zero and A_0 be Avogadro's number 6.023×10^{23} (atoms/mole). Then, with λ_0 being the decay constant specific to the parent radionuclide,

$$\frac{dN_0}{dt} = -\lambda_0 N_0, \; N_0(0) \text{ prescribed.} \qquad \left(\frac{\#\text{atoms}}{cm^3 - sec}\right) \qquad \text{(B.1)}$$

Multiplication of both sides of equation B.1 by $\frac{M_0}{A_0}$ yields

$$\frac{d\left(\frac{M_0 N_0}{A_0}\right)}{dt} = -\lambda_0 \left(\frac{M_0 N_0}{A_0}\right) . \qquad \left(\frac{gm}{cm^3 - sec}\right) \qquad \text{(B.2)}$$

Since the chemical mass of parent radionuclide in the volume V_0 is $C_0 = \frac{M_0 N_0}{A_0}$,

$$\frac{dC_0}{dt} = -\lambda_0 C_0 . \qquad \left(\frac{gm}{cm^3 - sec}\right) \qquad \text{(B.3)}$$

Multiplication by V_0 yields

$$\frac{d(V_0 C_0)}{dt} = -\lambda_0 (V_0 C_0) \qquad \left(\frac{gm}{sec}\right) \qquad \text{(B.4)}$$

or, in terms of parent radionuclide mass m_0,

$$\frac{dm_0}{dt} = -\lambda_0 m_0 \quad . \qquad \left(\frac{gm}{sec}\right) \qquad (B.5)$$

Integration obtains

$$m_0(t) = m_0(0)\, e^{-\lambda_0 t}, \quad t \geq 0, \quad m_0(0) = \text{initial mass (gm) of radionuclide "0".} \qquad (B.6)$$

N_1, the second radionuclide (first daughter) in the chain, is treated similarly so that

$$\frac{dN_1}{dt} = \lambda_0 N_0 - \lambda_1 N_1, \quad N_1(0) = 0 \quad . \qquad \left(\frac{\#\,atoms}{cm^3 - sec}\right) \qquad (B.7)$$

Multiplication of both sides of equation B.7 by $\frac{M_1}{A_0}$ yields

$$\frac{d\left(\frac{M_1 N_1}{A_0}\right)}{dt} = \lambda_0 \left(\frac{M_1}{M_0}\right)\left(\frac{M_0 N_0}{A_0}\right) - \lambda_1 \left(\frac{M_1 N_1}{A_0}\right) \qquad \left(\frac{gm}{cm^3 - sec}\right) \qquad (B.8)$$

or in terms of chemical concentration

$$\frac{dC_1}{dt} = \lambda_0 \left(\frac{M_1}{M_0}\right) C_0 - \lambda_1 C_1 \qquad \left(\frac{gm}{cm^3 - sec}\right) \qquad (B.9)$$

or in terms of chemical mass

$$\frac{dm_1}{dt} = \lambda_0 \left(\frac{M_1}{M_0}\right) m_0 - \lambda_1 m_1, \quad m_1(0) = 0 \quad . \qquad \left(\frac{gm}{sec}\right) \qquad (B.10)$$

By direct analogy for, k = 1, 2, 3 . . . , we can find for the kth radionuclide in the cascade chain

$$\frac{dm_k}{dt} = \lambda_{k-1} \left(\frac{M_k}{M_{k-1}}\right) m_{k-1} - \lambda_k m_k, \quad m_k(0) = 0 \quad . \qquad \left(\frac{gm}{sec}\right) \qquad (B.11)$$

The solution of the system is readily obtained via Laplace transform methods. We have

$$L\{m_0(t)\} = \frac{m_0(0)}{s+\lambda_0} \quad . \tag{B.12}$$

Furthermore,

$$L\left\{\frac{dm_k}{dt}\right\} = s\overline{m}_k(s) - m_k(0^+) = \lambda_{k-1}\left(\frac{M_k}{M_{k-1}}\right)\overline{m}_{k-1}(s) - \lambda_k\,\overline{m}_k(s) \quad . \tag{B.13}$$

Combining like terms obtains

$$(s+\lambda_k)\,\overline{m}_k(s) = \lambda_{k-1}\left(\frac{M_k}{M_{k-1}}\right)\overline{m}_{k-1}(s) \quad . \tag{B.14}$$

Solving for $\overline{m}_k(s)$,

$$\overline{m}_k(s) = \lambda_{k-1}\left(\frac{M_k}{M_{k-1}}\right)\frac{\overline{m}_{k-1}(s)}{s+\lambda_k} \quad . \tag{B.15}$$

Writing out the first few terms in this recursive formula obtains

$$\overline{m}_0(s) = \frac{m_0(0)}{s+\lambda_0} \quad , \tag{B.16}$$

$$\overline{m}_1(s) = \lambda_0\left(\frac{M_1}{M_0}\right)\frac{m_0(0)}{s+\lambda_0}\cdot\frac{1}{s+\lambda_k} \quad , \tag{B.17}$$

$$\overline{m}_2(s) = \lambda_1\left(\frac{M_2}{M_1}\right)\frac{m_1(s)}{s+\lambda_2} = \frac{\lambda_1\left(\frac{M_2}{M_1}\right)\lambda_0\left(\frac{M_1}{M_0}\right)m_0(0)}{(s+\lambda_0)(s+\lambda_1)(s+\lambda_2)} = \frac{\lambda_0\,\lambda_1\left(\frac{M_2}{M_0}\right)m_0(0)}{(s+\lambda_0)(s+\lambda_1)(s+\lambda_2)} \quad , \tag{B.18}$$

$$\overline{m}_3(s) = \lambda_2 \left(\frac{M_3}{M_2}\right) \frac{m_2(s)}{s+\lambda_3} = \frac{\lambda_0 \lambda_1 \lambda_2 \left(\frac{M_3}{M_0}\right) m_0(0)}{(s+\lambda_0)(s+\lambda_1)(s+\lambda_2)(s+\lambda_3)} \quad , \tag{B.19}$$

and in general

$$\overline{m}_k(s) = \lambda_{k-1} \left(\frac{M_k}{M_{k-1}}\right) \frac{\overline{m}_{k-1}(s)}{s+\lambda_k} = \frac{\lambda_0 \lambda_1 \lambda_2 \ldots \lambda_{k-1} \left(\frac{M_k}{M_0}\right) m_0(0)}{(s+\lambda_0)(s+\lambda_1)(s+\lambda_2)\ldots(s+\lambda_k)} \quad . \tag{B.20}$$

Using the inversion theorem and assuming that each λ_m is distinct obtains the general formula for

$$\begin{aligned} m_k(t) = \lambda_0\lambda_1\lambda_2 \ldots \lambda_{k-1} \left(\frac{M_k}{M_0}\right) m_0(0) \Bigg\{ & \frac{e^{-\lambda_0 t}}{(\lambda_1-\lambda_0)(\lambda_2-\lambda_0)(\lambda_3-\lambda_0)\ldots(\lambda_k-\lambda_0)} \\ & + \frac{e^{-\lambda_1 t}}{(\lambda_1-\lambda_0)(\lambda_2-\lambda_1)(\lambda_3-\lambda_1)\ldots(\lambda_k-\lambda_1)} \\ & + \frac{e^{-\lambda_2 t}}{(\lambda_0-\lambda_2)(\lambda_1-\lambda_2)(\lambda_3-\lambda_2)\ldots(\lambda_k-\lambda_2)} \\ & + \frac{e^{-\lambda_3 t}}{(\lambda_0-\lambda_3)(\lambda_1-\lambda_3)(\lambda_2-\lambda_3)(\lambda_4-\lambda_3)\ldots(\lambda_k-\lambda_3)} \\ & + \ldots + \frac{e^{-\lambda_k t}}{(\lambda_0-\lambda_k)(\lambda_1-\lambda_k)(\lambda_2-\lambda_k)\ldots(\lambda_{k-1}-\lambda_k)} \Bigg\} \quad , \end{aligned} \tag{B.21}$$

$$m_k(t) = \left(\frac{M_k}{M_0}\right) m_0(0) \left\{ \frac{\lambda_0 \lambda_1 \lambda_2 \ldots \lambda_{k-1} \, e^{-\lambda_0 t}}{\lambda_1 \left(1-\frac{\lambda_0}{\lambda_1}\right) \lambda_2 \left(1-\frac{\lambda_0}{\lambda_2}\right) \lambda_3 \left(1-\frac{\lambda_0}{\lambda_3}\right) \ldots \lambda_{k-1} \left(1-\frac{\lambda_0}{\lambda_{k-1}}\right) (\lambda_k - \lambda_0)} \right.$$

$$+ \frac{\lambda_0 \lambda_1 \lambda_2 \ldots \lambda_{k-1} \, e^{-\lambda_1 t}}{\lambda_0 \left(1-\frac{\lambda_1}{\lambda_0}\right) \lambda_2 \left(1-\frac{\lambda_1}{\lambda_2}\right) \lambda_3 \left(1-\frac{\lambda_1}{\lambda_3}\right) \ldots \lambda_{k-1} \left(1-\frac{\lambda_1}{\lambda_{k-1}}\right) (\lambda_k - \lambda_1)}$$

$$+ \frac{\lambda_0 \lambda_1 \lambda_2 \ldots \lambda_{k-1} \, e^{-\lambda_2 t}}{\lambda_0 \left(1-\frac{\lambda_2}{\lambda_0}\right) \lambda_1 \left(1-\frac{\lambda_2}{\lambda_1}\right) \lambda_3 \left(1-\frac{\lambda_2}{\lambda_3}\right) \ldots \lambda_{k-1} \left(1-\frac{\lambda_2}{\lambda_{k-1}}\right) (\lambda_k - \lambda_2)}$$

$$\left. + \ldots + \frac{\lambda_0 \lambda_1 \lambda_2 \ldots \lambda_{k-1} \, e^{-\lambda_k t}}{\lambda_0 \left(1-\frac{\lambda_k}{\lambda_0}\right) \lambda_1 \left(1-\frac{\lambda_k}{\lambda_1}\right) \lambda_2 \left(1-\frac{\lambda_k}{\lambda_2}\right) \ldots \lambda_{k-1} \left(1-\frac{\lambda_k}{\lambda_{k-1}}\right)} \right\}$$

(B.22)

or

$$m_k(t) = \left(\frac{M_k}{M_0}\right) m_0(0) \left\{ \frac{\lambda_0 \, e^{-\lambda_0 t}}{\left(1-\frac{\lambda_0}{\lambda_1}\right)\left(1-\frac{\lambda_0}{\lambda_2}\right)\left(1-\frac{\lambda_0}{\lambda_3}\right) \ldots \left(1-\frac{\lambda_0}{\lambda_{k-1}}\right)(\lambda_k - \lambda_0)} \right.$$

$$+ \frac{\lambda_1 \, e^{-\lambda_1 t}}{\left(1-\frac{\lambda_1}{\lambda_0}\right)\left(1-\frac{\lambda_1}{\lambda_2}\right)\left(1-\frac{\lambda_1}{\lambda_3}\right) \ldots \left(1-\frac{\lambda_1}{\lambda_{k-1}}\right)(\lambda_k - \lambda_1)}$$

$$+ \frac{\lambda_2 \, e^{-\lambda_2 t}}{\left(1-\frac{\lambda_2}{\lambda_0}\right)\left(1-\frac{\lambda_2}{\lambda_1}\right)\left(1-\frac{\lambda_2}{\lambda_3}\right)\ldots\left(1-\frac{\lambda_2}{\lambda_{k-1}}\right)(\lambda_k-\lambda_2)}$$

$$+\ldots+\frac{e^{-\lambda_k t}}{\left(1-\frac{\lambda_k}{\lambda_0}\right)\left(1-\frac{\lambda_k}{\lambda_1}\right)\left(1-\frac{\lambda_k}{\lambda_2}\right)\ldots\left(1-\frac{\lambda_k}{\lambda_{k-1}}\right)}\Bigg\} \quad , \qquad \text{(gm)} \qquad \text{(B.23)}$$

$k = 1, 2, 3\ldots$

Thus, for example

$$m_0(t) = m_0(0)\, e^{-\lambda_0 t} \quad , \qquad \text{(gm)} \qquad \text{(B.24)}$$

$$m_1(t) = \left(\frac{M_1}{M_0}\right) m_0(0) \left\{\frac{\lambda_0 \, e^{-\lambda_0 t}}{(\lambda_1-\lambda_0)} + \frac{e^{-\lambda_1 t}}{1-\frac{\lambda_1}{\lambda_0}}\right\} \quad , \qquad \text{(gm)} \qquad \text{(B.25)}$$

$$m_2(t) = \left(\frac{M_2}{M_0}\right) m_0(0) \left\{\frac{\lambda_0 \lambda_1 \, e^{-\lambda_0 t}}{(\lambda_1-\lambda_0)(\lambda_2-\lambda_0)} + \frac{\lambda_0 \lambda_1 \, e^{-\lambda_1 t}}{(\lambda_0-\lambda_1)(\lambda_2-\lambda_1)} + \frac{\lambda_0 \lambda_1 \, e^{-\lambda_2 t}}{(\lambda_0-\lambda_2)(\lambda_1-\lambda_2)}\right\} =$$

$$\left(\frac{M_2}{M_0}\right) m_0(0) \left\{\frac{\lambda_0 \, e^{-\lambda_0 t}}{\left(1-\frac{\lambda_0}{\lambda_1}\right)(\lambda_2-\lambda_0)} + \frac{\lambda_1 \, e^{-\lambda_1 t}}{\left(1-\frac{\lambda_1}{\lambda_0}\right)(\lambda_2-\lambda_1)} + \frac{e^{-\lambda_2 t}}{\left(1-\frac{\lambda_2}{\lambda_0}\right)\left(1-\frac{\lambda_2}{\lambda_1}\right)}\right\} \quad \text{(gm)} \, ,$$

(B.26)

$$m_3(t) = \left(\frac{M_3}{M_0}\right) m_0(0)\left\{\frac{\lambda_0\,\lambda_1\,\lambda_2\,e^{-\lambda_0 t}}{(\lambda_1-\lambda_0)(\lambda_2-\lambda_0)(\lambda_3-\lambda_0)} + \frac{\lambda_0\,\lambda_1\,\lambda_2\,e^{-\lambda_1 t}}{(\lambda_0-\lambda_1)(\lambda_2-\lambda_1)(\lambda_3-\lambda_1)}\right.$$

$$\left. + \frac{\lambda_0\,\lambda_1\,\lambda_2\,e^{-\lambda_2 t}}{(\lambda_0-\lambda_2)(\lambda_1-\lambda_2)(\lambda_3-\lambda_2)} + \frac{\lambda_0\,\lambda_1\,\lambda_2\,e^{-\lambda_3 t}}{(\lambda_0-\lambda_3)(\lambda_1-\lambda_3)(\lambda_2-\lambda_3)}\right\} =$$

$$\left(\frac{M_3}{M_0}\right) m_0(0)\left\{\frac{\lambda_0\,e^{-\lambda_0 t}}{\left(1-\frac{\lambda_0}{\lambda_1}\right)\left(1-\frac{\lambda_0}{\lambda_2}\right)(\lambda_3-\lambda_0)} + \frac{\lambda_1\,e^{-\lambda_1 t}}{\left(1-\frac{\lambda_1}{\lambda_0}\right)\left(1-\frac{\lambda_1}{\lambda_2}\right)(\lambda_3-\lambda_1)}\right.$$

$$\left. + \frac{\lambda_2\,e^{-\lambda_2 t}}{\left(1-\frac{\lambda_2}{\lambda_0}\right)\left(1-\frac{\lambda_2}{\lambda_1}\right)(\lambda_3-\lambda_2)} + \frac{e^{-\lambda_3 t}}{\left(1-\frac{\lambda_3}{\lambda_0}\right)\left(1-\frac{\lambda_3}{\lambda_1}\right)\left(1-\frac{\lambda_3}{\lambda_2}\right)}\right\} \text{ (gm) ,}$$

(B.27)

and

$$m_4(t) = \left(\frac{M_4}{M_0}\right) m_0(0)\left\{\frac{\lambda_0\,e^{-\lambda_0 t}}{\left(1-\frac{\lambda_0}{\lambda_1}\right)\left(1-\frac{\lambda_0}{\lambda_2}\right)\left(1-\frac{\lambda_0}{\lambda_3}\right)(\lambda_4-\lambda_0)}\right.$$

$$+ \frac{\lambda_1\,e^{-\lambda_1 t}}{\left(1-\frac{\lambda_1}{\lambda_0}\right)\left(1-\frac{\lambda_1}{\lambda_2}\right)\left(1-\frac{\lambda_1}{\lambda_3}\right)(\lambda_4-\lambda_1)} + \frac{\lambda_2\,e^{-\lambda_2 t}}{\left(1-\frac{\lambda_2}{\lambda_0}\right)\left(1-\frac{\lambda_2}{\lambda_1}\right)\left(1-\frac{\lambda_2}{\lambda_3}\right)(\lambda_4-\lambda_2)}$$

$$\left. + \frac{\lambda_3\,e^{-\lambda_3 t}}{\left(1-\frac{\lambda_3}{\lambda_0}\right)\left(1-\frac{\lambda_3}{\lambda_1}\right)\left(1-\frac{\lambda_3}{\lambda_2}\right)(\lambda_4-\lambda_3)} + \frac{e^{-\lambda_4 t}}{\left(1-\frac{\lambda_4}{\lambda_0}\right)\left(1-\frac{\lambda_4}{\lambda_1}\right)\left(1-\frac{\lambda_4}{\lambda_2}\right)\left(1-\frac{\lambda_4}{\lambda_3}\right)}\right\} \text{ (gm) .}$$

(B.28)

APPENDIX C

RADON-222 MODEL

This appendix describes a simple model that predicts the concentration of radon-222 progeny and the potential alpha energy concentration in a structure built on a disposal cell cap. Potential alpha energy concentration is used to calculate committed effective dose equivalents (H_E). Because of the short half-life of radon and its progeny, committed dose equivalents can be expected to be equal to annual effective dose equivalents.

Radon-222 gives rise to an eight-member serial decay-chain that ends with stable lead-206 as described in Table C.1. Radon is an inert noble gas that is not significantly accumulated in the body by any chemical or physical processes. Radon progeny is formed as condensation nuclei. A variable fraction of the condensation nuclei become attached to the ambient aerosol. The attached and unattached fractions progeny are deposited in different regions of the respiratory tract when inhaled. It is the radioactive decay of the alpha emitting progeny polonium-218 and polonium-219 deposited in the lung, especially on the bronchial epithelium that is responsible for the absorbed dose from radon. It is the unattached progeny that is deposited on the bronchial epithelium in the greatest quantities (NRC 1988). Radon-222 delivers a small fraction of the dose, except in unusual cases where the progeny is present at less than 10% of the equilibrium activity concentration (ICRP 1981). Of the progeny, those members below polonium-214 are not important because the 22-year half-life of lead-210 precludes significant ingrowth during the relatively short residence times of the particulates in the atmosphere. Polonium-214 can be assumed to be in secular equilibrium with bismuth-214 and its concentration need not be calculated directly. Therefore, the intake of polonium-218, lead-214, and bismuth-214 must be calculated to determine the dose.

The model assumes that radon-222 occurs in outdoor air and indoor air at concentrations equal to those predicted by the CASCADR8 model for soil-pore-gas at

Table C.1 Radon-222 Decay-Chain

Radionuclide		Half-Life	Yield	Decay Mode
radon-222	Rn-222	3.8 d	100%	alpha
polonium-218	Po-218	3.05 m	100%	alpha
lead-214	Pb-214	26.8 m	100%	beta
bismuth-214	Bi-214	19.7 m	100%	beta
polonium-214	Po-214	1.6 E-4 s	100%	alpha
lead-210	Pb-210	22 y	100%	beta
bismuth-210	Bi-210	5.0 d	100%	beta
polonium-210	Po-210	138 d	100%	alpha
lead-206	Pb-206	Stable		———

the surface (z=0). This is the most conservative assumption possible. Radon-222 enters houses primarily though advection of soil-pore-gas through imperfections in the foundation (Nazaroff 1992). In reality, soil-pore-gas emanating to the atmosphere or into a house will be diluted by air with a lower concentration of radon. However, it was concluded that parameterization of a model that considered these dilution processes was not possible at this time.

The concentration of radon-222 in soil-pore-gas as predicted by CASCADR8 is assumed to be proportional to the concentration of radium-226 in the buried waste. This constant of proportionality (k_S) is derived from CASCADR8 results based on the highest concentration predicted. The k_S factor does not vary with time, therefore, the concentration does not change in time with atmospheric pressure. However, the concentration of radon-222 in outdoor and indoor air will increase over time as radium-226 ingrows from thorium-230. The constant of proportionality k_s is specific for a given burial geometry.

The rate of change of the number of atoms of thorium-230 and radium-226 per volume of waste over time is

$$\frac{dN_0}{dt} = -\lambda_0 N_0 \qquad (C.1)$$

$$\frac{dN_1}{dt} = \lambda_0 N_0 - \lambda_1 N_1 \qquad (C.2)$$

where

N_0, N_1 = atom concentration of thorium-230 and radium-226 in waste, and

λ_0, λ_1 = thorium-230 and radium-226 radioactive decay constants

The solutions of equations C.1 and C.2 for the case where at t=0, $N_0 = N_0(0)$ and $N_1 = 0$ is well known as

$$N_0(t) = N_0(0)\, e^{-\lambda_0 t} \qquad (C.3)$$

$$N_1(t) = \frac{\lambda_0 N_0(0)\left(e^{-\lambda_0 t} - e^{-\lambda_1 t}\right)}{\lambda_1 - \lambda_0} \qquad (C.4)$$

Assuming that the radon-222 concentration is proportional to the radium-226 activity concentration in waste and converting equation C.4 to activity gives an expression for the radon-222 air concentration as a function of time as below.

$$A_2(t) = \frac{k_S \lambda_1 A_0(0)\left(e^{-\lambda_0 t} - e^{-\lambda_1 t}\right)}{\lambda_1 - \lambda_0} \qquad (C.5)$$

where

A_2 (t) = radon-222 activity concentration in indoor air, and

A_0 (0) = initial activity concentration of thorium-230 in waste

Since radon progeny seldom reach equilibrium in indoor air, an equilibrium factor of 0.4 was assumed based on NCRP (1987) estimates. Therefore, the activity concentration of the progeny in indoor air is given by

$$A_3 = A_4 = A_5 = 0.4\, A_2(t) \qquad (C.6)$$

where

A_3, A_4, A_5 = activity concentration of polonium-218, lead-214, and bismuth-214.

The potential alpha energy concentration in units of working levels (WL) at time t can be calculated as

$$WL(t) = 1.05 \times 10^{-3} A_3 + 5.16 \times 10^{-3} A_4 + 3.79 \times 10^{-3} A_5 \quad \text{(C.7)}$$

where the activity concentrations (A_3, A_4, A_5) are in units of pCi/l. Since the activity concentration of radon-222 and its progeny will be controlled by the decay of thorium-230 and ingrowth of radium-226, in any given yearly interval the change in the radon concentration will be small. If the radon-222 concentration is assumed to be constant in each given year and the intruder is indoors 100% of the time, the total annual cumulative exposure in working level months is

$$WLM = 51.6 \times WL(T) \quad . \quad \text{(C.8)}$$

Where 51.6 is the number of 170 hour working months in one year of continuous exposure. The committed effective dose equivalent (H_E) for any given year of intake is then

$$H_E = < H_E/WLM > \times WLM \quad \text{(C.9)}$$

where

$< H_E \backslash WLM >$ = Dose conversion factor for reference man.

REFERENCES

Atomic Energy Act of 1954, U.S. Code.

Barker, L. 1992. Private communications.

Bateman, H. 1910. The solution of a system of differential equations occurring in the theory of radioactive transformations. proc. cambridge philos. 15cv: pp 423-427.

Cawlfield, D. E., F. T. Lindstrom, D. F. Emer, G. J. Shott, and M. E. Donahue. 1992. CASCADER: An m-chain gas-phase radionuclide transport and fate model. Volume 2 - Users Guide. DOE/NV/10630-57. Reynolds Electrical & Engineering Co., Inc. P.O. Box 98521, Las Vegas, NV.

ICRP 1975. International council on radiological protection, report of the task group on reference man, ICRP Publication 23, Pergamon Press, New York.

ICRP 1979. Limits for intake of radionuclides by workers, ICRP Publication 30. Annals of the ICRP, Vol 2, No 319.

ICRP 1981. International council on radiological protection, limits for inhalation of radon daughters by workers, ICRP Publication 32, Annals of the ICRP (6) No. 1.

Lindstrom, F. T., D. E. Cawlfield, D. F. Emer, G. J. Shott, and M. E. Donahue. 1992c. A simulation of the transport and fate of radon-220 derived from thorium-232 low-level waste in the near-surface zone of the radioactive waste management site in area 5 of the nevada test site. DOE/NV/10630-38. Reynolds Electrical & Engineering Co., Inc. P.O. Box 98521, Las Vegas, NV.

Lindstrom, F. T., D. E. Cawlfield, D. F. Emer, G. J. Shott, and M. E. Donahue. 1992a. CASCADER: An m-chain gas-phase radionuclide transport and fate model. Volume 1-basic physics and mathematics. DOE/NV/10630-23. Reynolds Electrical & Engineering Co., Inc. P.O. Box 98521, Las Vegas, NV.

Lindstrom, F. T., D. E. Cawlfield, D. F. Emer, G. J. Shott, and M. E. Donahue. 1992b. CASCADER: An m-chain gas-phase radionuclide transport and fate model. Volume 3-heterogeneous layered porous media. DOE/NV/10630-41 Reynolds Electrical & Engineering Co., Inc. P.O. Box 98521, Las Vegas, NV.

National Research Council. Committee on the biological effects of Ionizing radiation. Health risks of radon and other internally deposited alpha-emitters. BIER IV. National Academy Press, Washington, DC.

NCRP 1987. Exposure of the population in the United States and Canada from natural background radiation. NCRP Report 94, Bethesda, MD.

NCRP 1988. Measurement of radon and radon daughters in air. NCRP Report 97, Bethesda, MD.

Nazaroff, W. W. 1992. Radon transport from soil to air. Reviews of Geophysics, 30 (2), pp 137-160.

U.S. Department of Energy Order 5820.2A, Radioactive Waste Management, Washington, DC. 1988.

U.S. Environmental Protection Agency. Code of Federal Regulations. Washington, D.C., U.S. Government Printing Office; 40 CFR 61, 1990.

DISTRIBUTION LIST

Waste Management Department Reference Library, Reynolds Electrical & Engineering Co., Inc. P.O. Box 98521, M/S 501, Las Vegas, NV 89193. (20)

F. T. Lindstrom, Reynolds Electrical & Engineering Co., Inc. P.O. Box 98521, M/S 738, Las Vegas, NV 89193. (5)

D. E. Cawlfield, Reynolds Electrical & Engineering Co., Inc. P.O. Box 98521, M/S 738, Las Vegas, NV 89193. (5)

D. F. Emer, Reynolds Electrical & Engineering Co., Inc. P.O. Box 98521, M/S 738, Las Vegas, NV 89193. (5)

G. J. Shott, Reynolds Electrical & Engineering Co., Inc. P.O. Box 98521, M/S 738, Las Vegas, NV 89193. (5)

T. M. Hayes, Reynolds Electrical & Engineering Co., Inc. P.O. Box 98521, M/S 551, Las Vegas, NV 89193. (2)

DOE Office of Scientific and Technical Information, U.S. Department of Energy, P.O. Box 98518, M/S 505, Las Vegas, NV 89193. (2)

DOE/NV Technical Information Resource Center, U.S. Department of Energy, P.O. Box 98518, M/S 505, Las Vegas, NV 89193. (2)

DATE

FILMED

4/18/94

END